Appendix D.3

Redundancy Analysis of I-Girder Superstructures under Vertical Loads

By Jian Yang, Feng Miao and Michel Ghosn

Contents

Redundancy Analysis of I-Girder Superstructures under Vertical Loads

by

Jian Yang, Feng Miao and Michel Ghosn

Abstract

This report performs the sensitivity analysis for typical steel I-girder superstructures subjected to vertical loads simulating the effect of truck traffic. The base case configuration is a three-span continuous steel I-girder bridge superstructure consisting of six composite girders. Simple span variations on the original bridge are analyzed in this Report. Simple span bridges with different spans are also designed and analyzed. The superstructures are loaded by two HS-20 trucks and the loads are incremented until the bridge superstructure system fails. The sensitivity analysis is performed to study how variations in the bridge geometry, member properties and loading conditions affect the redundancy of the superstructure and to investigate the differences in the behavior between continuous bridges and simple span bridges. Specifically, the Nonlinear Static Pushdown Analysis (NSPA) is used to investigate the sensitivity of the structure to various parameters including: a) changes in the resistance of the longitudinal members; b) plastic hinge length of the girders; c) number of trucks and loading positions; d) span length configuration of 3-span continuous bridges; e) span length variation of simple span bridges; f) the presence of bracing; g) beam spacing and h) slab thickness.

The behavior of the bridge superstructure is analyzed using the SAP2000 Finite Element Analysis software. Load deformation curves are plotted for each variation in the bridge's properties and the ultimate load carrying capacities are compared to those of the basic bridge configuration. Based on the results obtained, it is observed that relatively moderate changes in the following parameters have generally minor effect on bridge redundancy: span length of simple bridges, plastic hinge length, bridge bracing and slab thickness. The parameters that seem to have the most effect include beam spacing which when increased leads to a decrease in bridge redundancy for the ultimate capacity and to a larger degree for the damaged bridge condition. Increasing the slab thickness can raise bridge redundancy ratio for the damaged condition. The effect of resistance over dead load ratio on the damaged bridge scenario is significant unlike what is observed for ultimate limit state condition. Side-by-side trucks in the middle span are most likely to control the redundancy of this multi-span bridge configuration. Higher redundancy ratios would be obtained if a single truck is loaded in each of two spans as compared to side-by-side trucks in each of two spans. For simple span bridges the effect of changes in the member resistance are insignificant as long as the beams maintain a margin of safety over the minimum resistance needed to carry the dead load.

1. Introduction

This technical report presents the results of the redundancy analysis of steel I-girder bridge superstructures subjected to vertical loads. The objective of the analysis is to supplement the results previously provided in NCHRP 406 particularly for continuous I-girder bridges. The basic bridge configuration selected for this set of analyses is a three-span continuous composite steel I-girder bridge with 50-ft-80-ft and 50-ft spans. A sensitivity analysis is performed to study the effect of variations in: a) the resistance capacity; b) plastic hinge length ; c) number of trucks and loading positions; d) span length configuration of 3-span continuous bridges; e) span length variation of simple span bridges; f) the presence of bracing; and g) spacing between beams;. The analyses performed in this report and those in are part of one row of the Matrix of bridge configurations that were set in the approved work plan. The list of parameters for I-girder bridges that were scheduled for analysis is summarized in Table 1.

This report compares the results of the sensitivity analysis for the new set of parameters and provides a preliminary evaluation of the results.

Table 1.1 Summary of I-girder configurations and analyses that are to be addressed in this NCHRP12-86 project.

Loading scenario	**Type of structure**	**Model**	**Spans**	**Design**	**Parametric analysis**	**Additional parameters**	**Damaged bridge scenario**
Vertical load on I-Girder bridges	• Steel I-girder • P/s I-girder	Fig. A	• Continuous 50-80-50 ft • Simple 80-ft	• Six beams at 8-ft spacing • Full continuity • Continuity for live load • Different depth/thickness ratios for steel sections in negative bending.	• Diaphragms of various stiffness • Resistance over dead load ratio • Effect of hinge in steel beam	• Number of beams • Beam spacing, • Span length **Use NCHRP 406**	• Remove external girder of one span

2. Structural Modeling

2.1 Base bridge model

The cross section of the basic bridge configuration which is an adaptation of the bridge tested by Burdette and Goodpasture (1971) is given in Fig. 2.1 that is modeled using the FEM model of Figure 2.2.

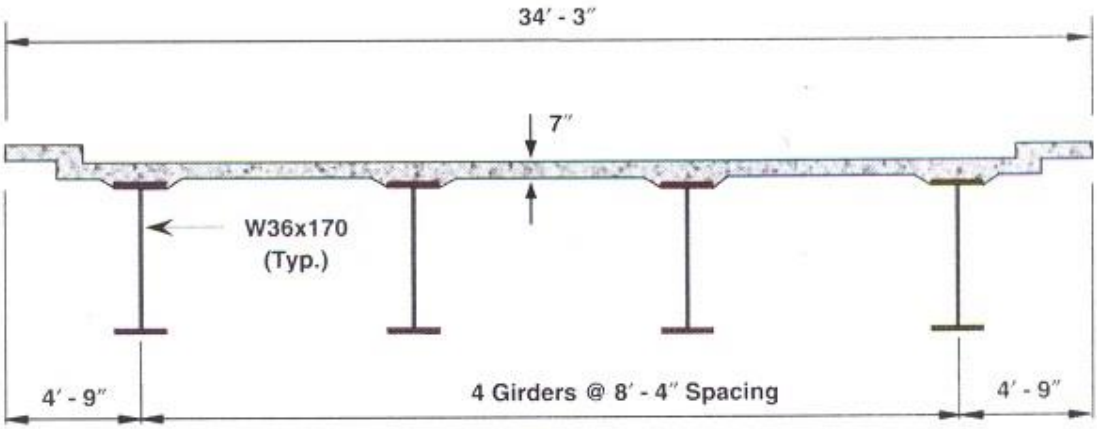

Figure 2.1 – Cross section of 3-span I-girder bridge.

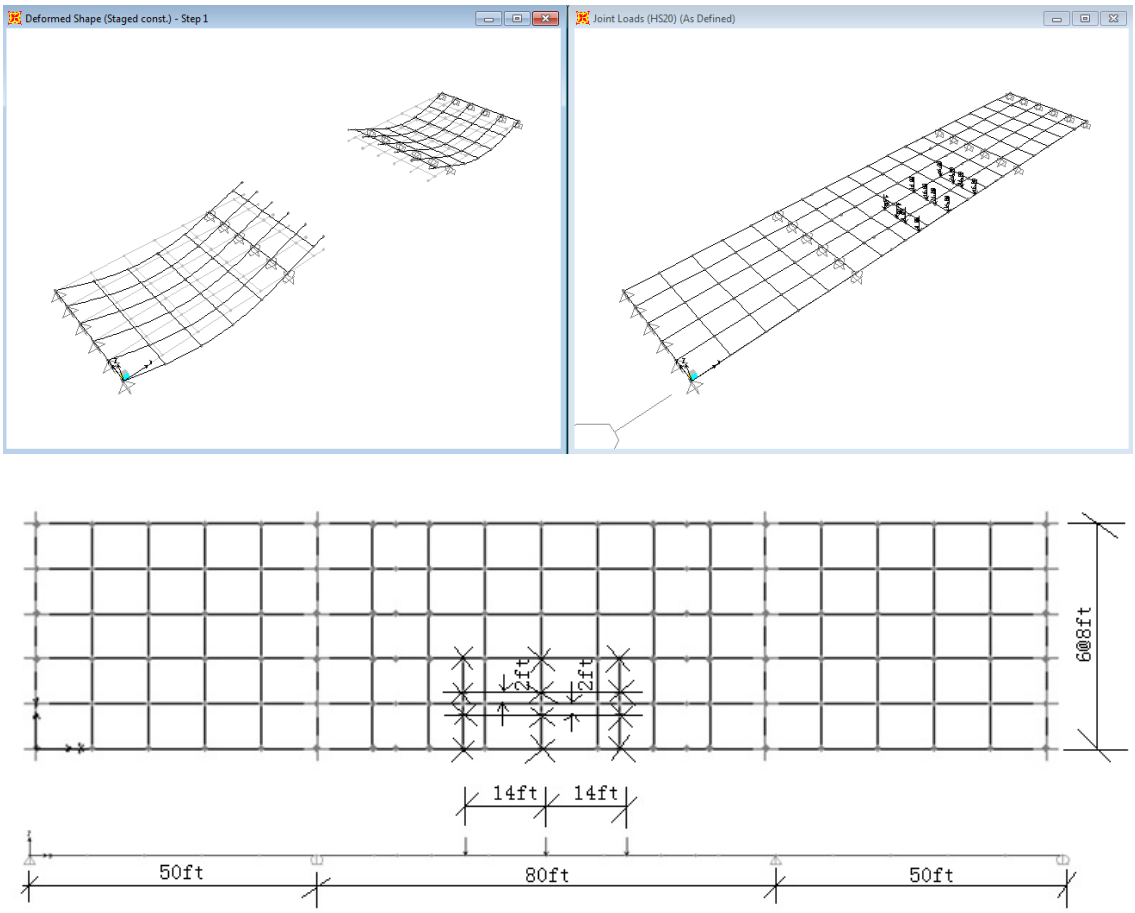

Figure 2.2 SAP2000 model of the 3-span continuous steel-I girder bridge

2.2 Pushdown analysis of basic bridge model

From the section analysis, the composite girder section is found to have an ultimate positive moment capacity equal to $R=M^{+}=49{,}730$ Kip-in (4,144 kip-ft). This value corresponds to the ultimate capacity of the composite beam as obtained from the actual stress-strain relationships of structural steel and the concrete during the calculation of the moment-curvature relationship.

Using the results of a linear elastic analysis, the positive moment due to the dead load at the mid-span of a girder is obtained as D=4,860 kip-in. The external girder will carry a linear elastic moment equal to 6,450 kip-in due to two side-by-side AASHTO HS-20 vehicles. If a traditional

linear elastic analysis is used to evaluate the load carrying capacity of the bridge, the number of HS-20 trucks that would lead to failure would be obtained from:

$$LF_1 = \frac{R - D}{DF_1 LL_{HS-20}} \tag{2.1}$$

Where R is the member's unfactored moment capacity, D is the member's unfactored dead load, DF_1 is the linear elastic distribution factor, and LL_{HS-20} is the total live load moment effect due to the HS-20 vehicles. For improved accuracy, the product $DF_1 LL_{HS-20}$ is obtained from the linear elastic results as the highest live load moment effect for any longitudinal member from the SAP2000 results rather than using the AASHTO load distribution factors.

Using Eq. (2.1) is consistent with traditional methods for evaluating the load carrying capacity of the bridge superstructure. In fact, LF_1 in Eq. (2.1) is similar to the Rating Factor R.F. used to assess the load rating of existing bridges. The difference between R.F. and LF_1 is that Eq. (2.1) ignores the load and resistance factors and considers only the static load. The load and resistance factors are not needed in this analysis because we are interested in evaluating as accurately as possible the load carrying capacity of the bridge superstructure rather than providing safe envelopes for design and load rating purposes. In this analysis, we express the load carrying capacity of the superstructure in terms of the multiples of the static HS-20 load that the bridge can safely carry. The dynamic impact factor is not needed because we are looking tat he resistance of the bridge and not the applied load.

For this particular bridge, with R=49,730 kip-in, D=4,860 kip-in and $DF_1 LL_{HS-20}$ =6,450 kip-in, the application of Eq. (2.1) indicates that the load factor that leads to first member failure in positive bending assuming traditional linear elastic analysis methods is LF_1=6.96. This result indicates that if one is to follow traditional bridge analysis methods, the first member of the bridge will reach its ultimate capacity at a load equal to 6.96 times the effect of two HS-20 trucks.

To check the negative bending, the calculation is repeated following the same process but where all the moments are evaluated for the girder section located over the interior support. In this

case, the negative moment capacity of the non-composite section of the bridge is $R = M^- = 42{,}000$ kip-in (3,500 kip-ft). This value corresponds to the ultimate capacity of the beam as obtained from the actual stress-strain relationship of structural steel during the calculation of the moment-curvature relationship shown in Figure 2.2. The negative moment due to the dead load at the interior support of a girder is obtained as $D^- = 2{,}809$ kip-in. The external girder section over the interior support will carry a linear elastic negative moment equal to 3,069 kip-in due to two side-by-side AASHTO HS-20 vehicles. According to Eq. (2.1), the load factor for first member failure due to negative bending is $LF_1 = 12.77 > 6.96$. This means that the positive bending controls the first member failure for the given loading scenario.

The next step of the analysis process consists of performing the nonlinear pushdown analysis for the superstructure. Figure 2.3 gives the total reactions versus the maximum vertical deflection of the bridge when a nonlinear incremental load analysis is performed. The results of the pushdown analysis are summarized in Table 2.1.

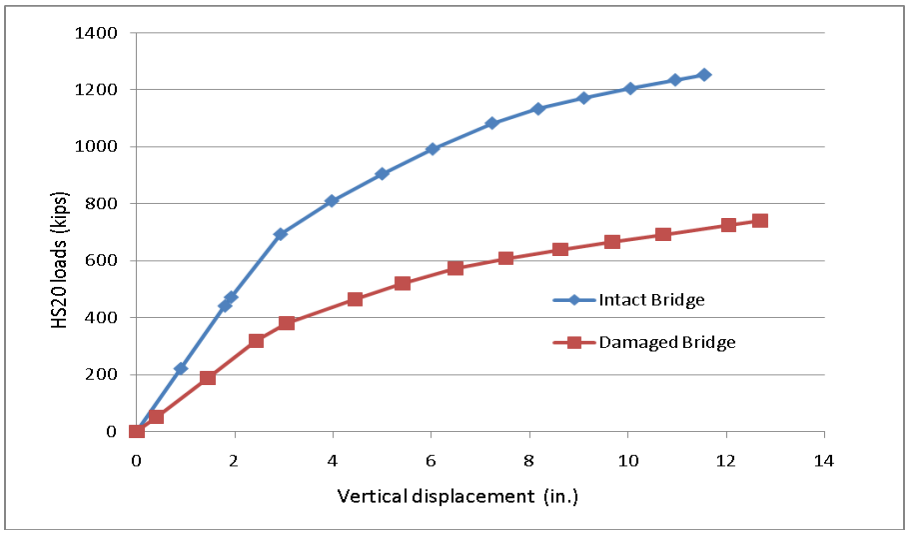

Figure 2.3 Load deflection relationship of basic 3-span steel bridge configuration

Table 2.1 Results of the pushdown analysis of basic 3-span steel bridge

3-span bridge	LF_1	LF_{300}	LF_{200}	LF_{100}	LF_u	LF_d
SAP2000	6.96	5.02	6.15	8.25	8.70	5.14

Figure 2.3 shows that the ultimate capacity is 1253 kips when the HS-20 vehicles are incremented by a factor, LF_u equals to 1253 kips/144 kips=8.70, as shown in Table 2.1. A displacement equal to span length/300 (3.2 in) is reached when the load factor, LF_{300} is equal to 722.9 kips/144 kips=5.02. A displacement equal to span length/200 (4.8 in) is reached when the loads are incremented by a factor, LF_{200}= 886.3 kips/144 kips=6.15. A displacement equal to span length/100 (9.6 in) is reached when the load factor reaches a value, LF_{100} equal to 1188.3 kips /144 kips =8.25.

To analyze the capacity of the bridge assuming that the external beam has been totally damaged due to an unexpected event such as an impact from a passing truck or a fracture of the steel, the analysis of the superstructure is performed after completely removing the exterior longitudinal beam but keeping the two side-by-side truck loads at the same position. The nonlinear pushdown analysis is executed after the damaged external longitudinal composite girder is removed from the mesh but the live load over the external longitudinal beam is transferred to the remaining undamaged girders through transverse beam elements representing the contributions of the slab. In this analysis, the removal of the external girder assumes that the dead load of the external girder is also removed.

The analysis of the damaged bridge reveals that the ultimate capacity of the damaged bridge is reached when the HS-20 vehicles are incremented by a factor LF_d equal to 740.6 kips /144 kips =5.14, as shown in Table 2.1.

2.3 Evaluation of bridge redundancy

According to NCHRP 406, redundancy is defined as the capability of a structure to continue to carry loads after the failure of the most critical member. The overall load-displacement response of the bridge can be represented as shown in Figure 2.4.

Figure 2.4 gives a conceptual representation of the behavior of a structure and the different levels that should be considered when evaluating member safety, system safety and system redundancy. For example, the solid line labeled "Intact system" may represent the applied load versus maximum vertical displacement of a ductile multi-girder bridge superstructure. In this case, the load is incremented to study the behavior of an "intact system" that was not previously subjected to any damaging load or event.

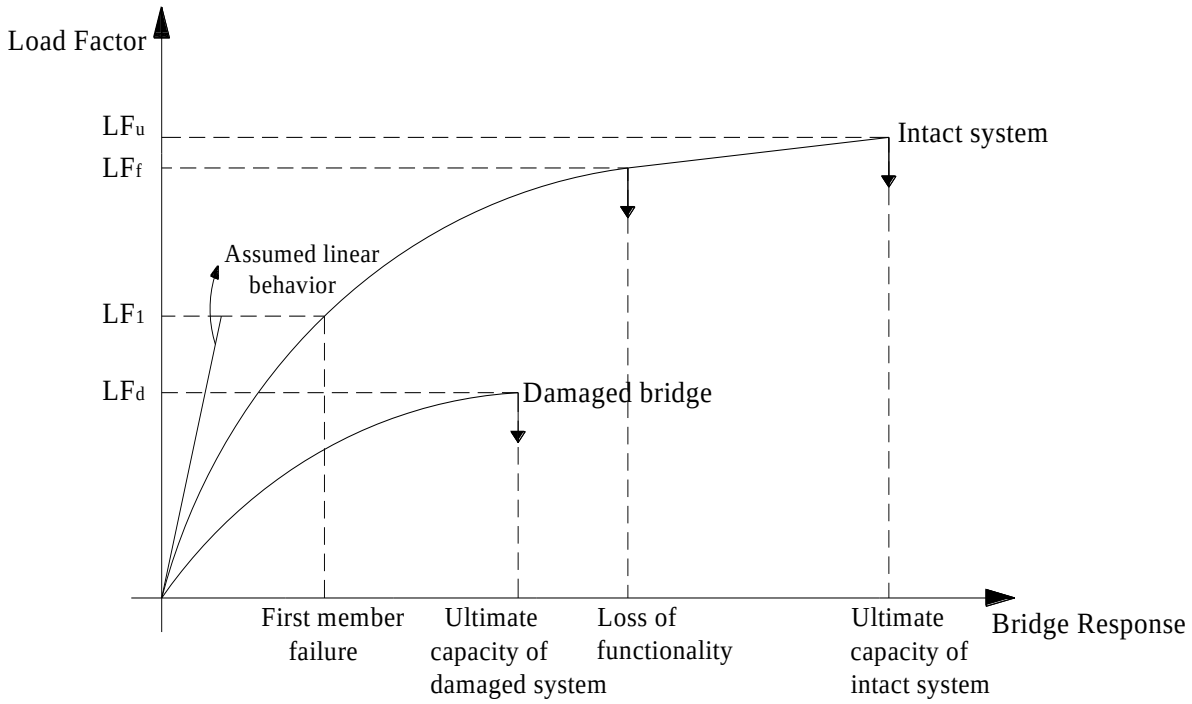

Figure 2.4 Representation of typical behavior of bridge systems

Assuming that the vertical live load applied has the configuration of the AASHTO HS-20 vehicle. The bridge is first loaded by the dead load and then the HS-20 load is applied. Usually, due to the presence of safety factors, no failure occurs after the application of the dead load plus the HS-20 load. The first structural member will fail when the HS-20 truck weight is multiplied by a factor LF_1. LF_1 would then be related to member safety. Note that if the bridge is under-designed or has major deficiencies, it is possible to have LF_1 less than 1.0. Generally, the

ultimate capacity of the whole bridge is not reached until the HS-20 truck weight is multiplied by a factor LF_u. LF_u would give an evaluation of system safety. Large vertical deformations rendering the bridge unfit for use are reached when the HS-20 truck weight is multiplied by a factor LF_f. LF_f gives a measure of system functionality. A bridge that has been loaded up to this point is said to have lost its functionality.

If the bridge has sustained major damage due to the brittle failure of one or more of its members, its behavior is represented by the curve labeled "damaged system". A damaged bridge may be a bridge that has lost one of its members due to a collision by a truck or due to major degradation of the member capacity due to corrosion. Other damage scenarios may include the failure of a member due to a fatigue fracture or if some extreme event led to shearing off of the member. In this case, the ultimate capacity of the damaged bridge is reached when the weight of the HS-20 truck is multiplied by a factor LF_d. LF_d would give a measure of the remaining safety of a damaged system.

For a structure that has not been previously subjected to a damaging event, the capacity of the superstructure to resist the first failure of a member as estimated using traditional analysis methods is represented by LF_1. Also, the ability of the "original undamaged superstructure", herein referred to as "intact superstructure", to continue to carry load even after one member reaches its capacity, is represented by the load factors LF_u. However, if a superstructure may become nonfunctional due to large displacements, its capacity may be represented by LF_{300}, LF_{200} or LF_{100}. In NCHRP 406, the functionality criterion was set in term of LF_{100} which is the load factor at which a displacement equal to span length/100 is reached.

Recently, some researchers have defined robustness as the capability of the system to carry some load after the brittle failure of a main load carrying member (see for example, Faber et al, 2008). According to NCHRP 406, the evaluation of system robustness is equivalent to evaluating the redundancy for the damaged system which is represented by the load factor LF_d.

If we accept the definition of redundancy as the capability of a structure to continue to carry loads after the failure of the most critical member, then comparing the load multipliers LF_u, LF_f,

LF_d to LF_1would provide non-subjective and quantifiable measures of system redundancy and robustness. Based on that logic, NCHRP 406 defines three deterministic measures of redundancy referred to as redundancy ratios or system reserve ratios which relate the system's capacity to the most critical member's "assumed" capacity:

$$R_u = \frac{LF_U}{LF_1}$$
$$R_f = \frac{LF_f}{LF_1} \qquad (2.2)$$
$$R_d = \frac{LF_d}{LF_1}$$

where R_u =redundancy ratio for the ultimate limit state, R_f=redundancy ratio for the functionality limit state, R_d= redundancy ratio for the damage condition.

The definitions provided in Eq. (2.2) originally provided for superstructures under vertical loads in NCHRP 406 were subsequently used for substructures systems under lateral load in NCHRP 458.

The redundancy ratios as defined in NCHRP 406 and 458 provide nominal deterministic measures of bridge redundancy (and robustness). For example, when the ratio R_u is equal to 1.0 (LF_u=LF_1), the ultimate capacity of the system is equal to the capacity of the bridge to resist failure of its most critical member. Based on the definitions provided above, such a bridge is nonredundant. As R_u increases, the level of bridge redundancy increases. A redundant bridge should also be able to function without leading to high levels of deformations as its members plasticize. Thus, R_f provides another measure of redundancy. Similarly, a redundant bridge structure should be able to carry some load after the brittle fracture of one of its members, and R_d would provide a quantifiable non-subjective measure of structural redundancy for the damaged bridge which has also been defined as robustness.

The NCHRP 406 criteria for bridge redundancy require that: a) the ratio of the ultimate system capacity to first member failure, R_u, should be equal or exceed 1.3; b) the ratio of the system capacity to resist a maximum vertical deflection of span length/100, defined as R_f, should be equal to or exceed 1.10 times the capacity of the bridge to resist first member failure; and c) that

a damaged system should have a system capacity equal to or exceeding 0.50 times the capacity of the intact system to resist first member failure ($R_d \geq 0.5$).

The criteria of NCHRP 406 were selected following the redundancy and reliability analysis of many bridge superstructures of different material, section type, span length, number of beams, and beam spacing. In keeping with traditional practice that classified bridges with four parallel I-girders as redundant, reliability and redundancy criteria were selected in NCHRP 406 so that they are met on the average by typical four-I-girder bridges. Possible adjustments to these criteria will be considered in this NCHRP 12-86 Project, if necessary, based on the additional results that this project will produce and in consultation with the Project Panel.

For the base case bridge superstructure system analyzed in this report, the redundancy ratios are obtained as:

$R_u = LF_u/LF_1 = 8.70/6.96 = 1.25 < 1.30$

$R_f = LF_f/LF_1 = 8.25/6.96 = 1.18 > 1.10$

$R_d = LF_d/LF_1 = 5.14/6.96 = 0.74 > 0.50$

That is if we are to maintain the same criteria set in NCHRP 406 this bridge would be considered nonredundant for the ultimate limit state even though it does satisfy the criteria for the functionality limit state and the damaged condition.

3. Parametric analysis

In this section we continue the parametric analysis that was initiated in Appendix A of the previous Quarterly Report. Specifically, in this report we review the effect of the results to the following parameters:

1. Effect of member resistance.
2. Effect of plastic hinge length
3. Effect of truck placement
4. Effect of span length
5. Effect of bracing
6. Effect of beam spacing

3.1 Effect of member resistance

The member resistance and the dead loads are important parameters for the evaluation of the load carrying capacity of the beams and bridge systems. The object of this section is to investigate the importance of these parameters on the redundancy ratios. Several scenarios are investigated in this section: 1) the member resistances of the continuous bridge are changed for both the positive bending and negative bending regions; 2) the positive bending capacities of the continuous bridge are changed; 3) the negative bending capacities are changed; 4) the cross sections are changedto use more realistic moment and curvature relationships; 5) the bending capacity of simple span bridges are changed to compare the effect of member resistance on continuous and simple span bridges.

3.1.1 Three-span continuous bridge

1) Positive and negative bending capacities of the three-span bridge are changed

Four cases are analyzed to investigate the effect of changes in the member resistances as follows:

Case 1: Capacity +10%, dead load keeps the same value;
Case 2: Capacity +20%, dead load keeps the same value;
Case 3: Capacity -25%, dead load keeps the same value;
Case 4: Capacity -50%, dead load keeps the same value.

The Moment curvature curves for Cases 1 through4 are compared to the base case for positive bending regions and negative bending regions as shown in Figure 3.1 and Figure 3.2, respectively. The load deflection curves for the Base case and Cases 1-4 are shown in Figure 3.3. The redundancy ratios are summarized in Table 3.1. The effect of the capacity ratio on redundancy ratio is illustrated in Figure 3.4.

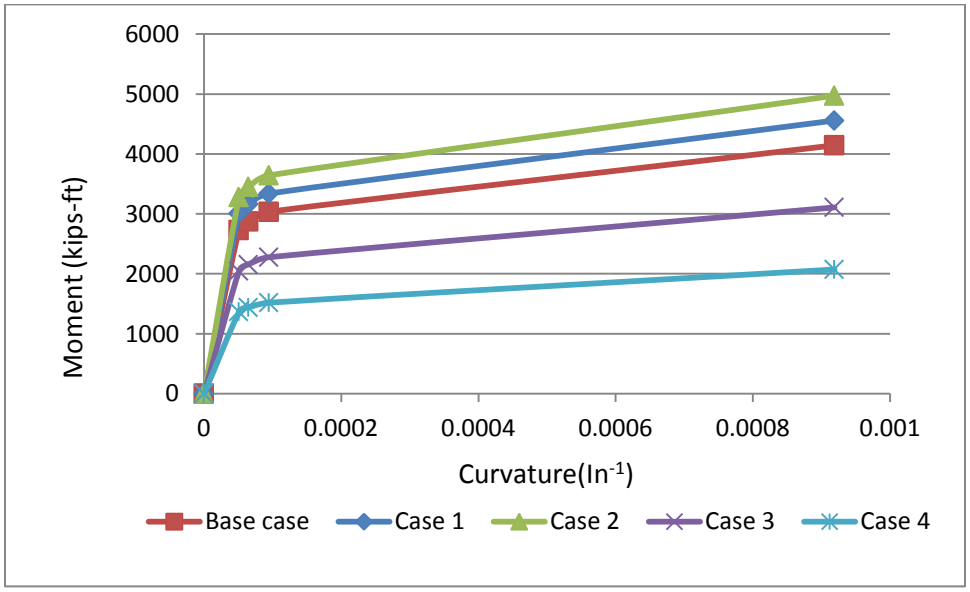

Figure 3.1 M-phi curves for composite steel I girders for the Base case and Case 1-4 for positive moment

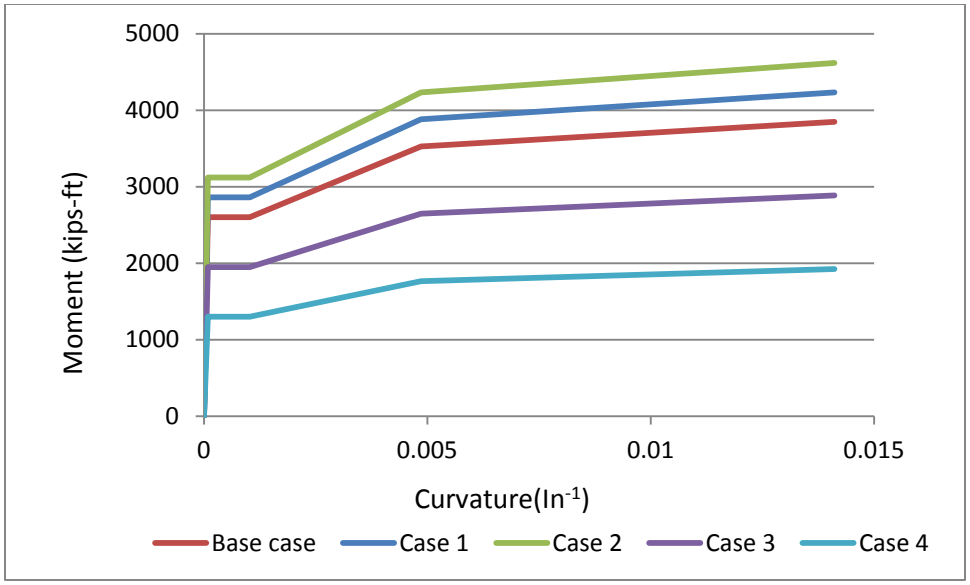

Figure 3.2 M-phi curves for composite steel I girders for the Base case and Cases 1-4 for negative moment

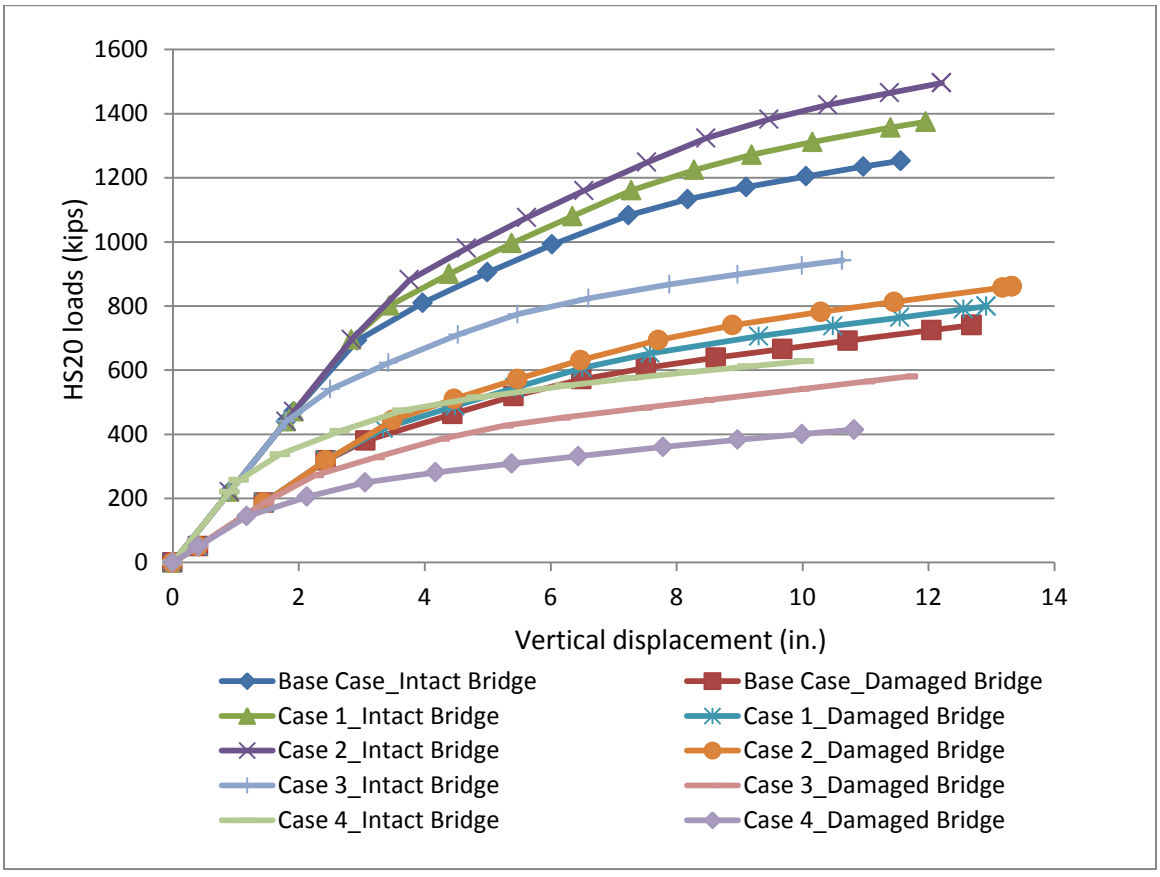

Figure 3.3 Load deflection curves for different resistance values

Table 3.1 Comparison of results of redundancy analysis for different resistance values

3-span bridge	LF_1*	LF_{300}	LF_{200}	LF_{100}	LF_u	LF_d	R_{f100}	R_u	R_d**
Base case	6.96	5.02	6.15	8.25	8.70	5.14	1.18	1.25	0.74
Case 1	7.73	5.27	6.53	8.95	9.55	5.55	1.16	1.24	0.72
Case 2	8.50	5.34	6.90	9.64	10.39	5.67	1.14	1.22	0.67
Case 3	5.03	4.18	5.06	6.36	6.55	4.03	1.26	1.30	0.80
Case 4	3.10	3.09	3.57	4.31	4.36	2.88	1.39	1.41	0.93

Note: * The value of LF_1 is the minimum load factor of positive bending moment and negative bending moment failure. All cases were governed by positive bending ** In this report, the weight of the damaged beam is removed in the damage scenario unless it is specified..

From Table 3.1, it is observed that the load factors, LF_1, and LF_u in Cases 1-2 increase by approximately the same percentage as that of the member's moment capacities increase. For this particular three-span continuous bridge, LF_1 increases by 11% and 22% for Case 1 and Case 2, respectively, compared to that of the base case. Also, LF_u increases by 10% and 19% for Case 1 and Case 2, respectively. LF_d increases by 8% and 10% for Case 1 and Case 2, respectively. Thus, the redundancy ratio R_u for the ultimate limit state decreases by about 2% while the redundancy ratio R_d for the damage condition decreases by about 9%.

When the member capacities are reduced by 25% and 50% for Case 3 and Case 4, respectively, the redundancy ratio for the ultimate limit state, R_u increases by 4% and 13% for Case 3 and Case 4, respectively. The redundancy ratio for the damage condition, R_d increases by 8% and 26% for Case 3 and Case 4, respectively.

It is concluded that variations of the redundancy ratio R_u are about ¼ of the variations in the members' resistances in the opposite direction, while the changes in R_d are within 50% of the changes in the members' capacities. These observations can be visualized in the plots of Figure 3.4 using four different resistance capacities of the bridge girders, that is, C/Cb=0.5, 0.75, 1.1 and 1.2.

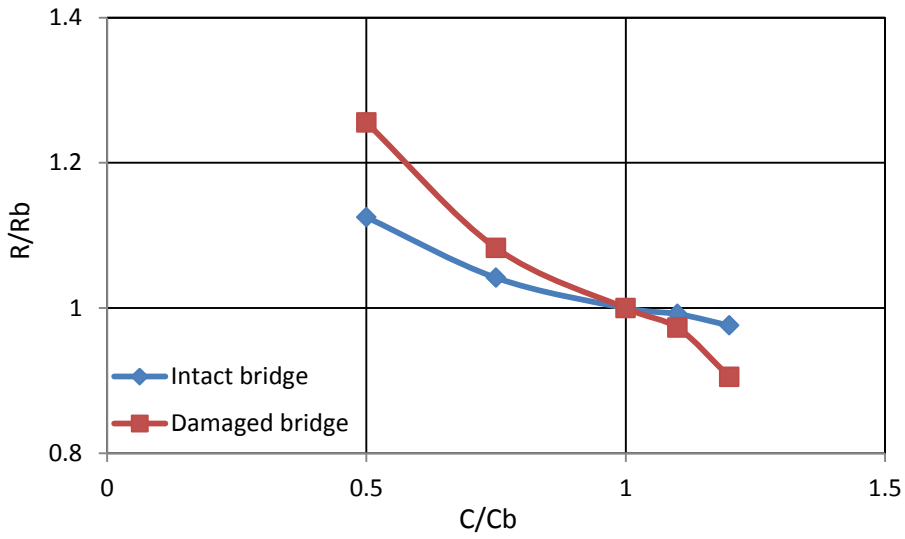

Figure 3.4 Effect of capacity ratio on redundancy ratio results

2) Only positive bending moment is changed.

Four cases are analyzed to investigate the effect of changes in the positive moment capacities only. The cases are listed as:

Case 1: Change positive moment capacity only by+10%;
Case 2: Change positive moment capacity only by+20%;
Case 3: Change positive moment capacity only by -25%;
Case 4: Change positive moment capacity only by-50%.

The load deflection curves for the Base case and Cases 1 through4 are shown in Figure 3.5. The redundancy ratios are summarized in Table 3.2. The effects of changes in the member capacities on the redundancy ratios are plotted in Figure 3.6.

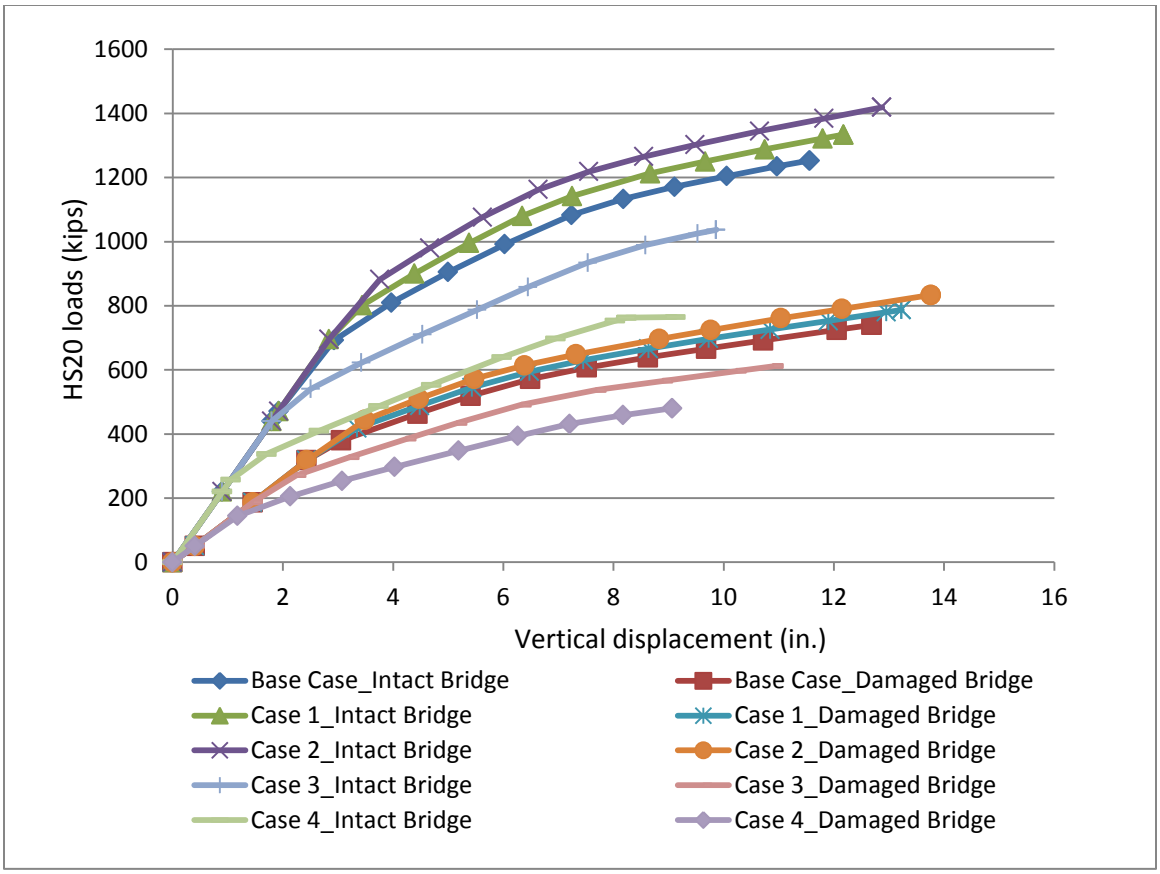

Figure 3.5 Load deflection curves for different positive resistance values

Table 3.2 Comparison of results of redundancy analysis of various positive resistance values

3-span bridge	LF_1*	LF_{300}	LF_{200}	LF_{100}	LF_u	LF_d	R_{f100}	R_u	R_d
Base case	6.96	5.02	6.15	8.25	8.70	5.14	1.18	1.25	0.74
Case 1	7.73	5.27	6.53	8.66	9.26	5.47	1.12	1.20	0.71
Case 2	8.50	5.34	6.90	9.07	9.85	5.79	1.07	1.16	0.68
Case 3	5.03	4.18	5.08	7.14	7.20	4.25	1.42	1.43	0.85
Case 4	3.10	3.12	3.89	--**	5.31	3.34	--**	1.71	1.08

Note: : * The value of LF_1 is the minimum load factor of positive bending moment and negative bending moment failure. All cases were governed by positive bending.

** The bridge reaches its ultimate limit before the displacement reaches L/100.

As expected, Table 3.2 shows that the load factors, LF_1, LF_u and LF_d increase due to stronger positive member capacity. However, the redundancy ratios decrease while the resistance capacity increases. In other words, a stronger positive member capacity leads to lower redundancy ratios. This is because stronger resistances of bridge girders have a more significant effect on LF_1 than

LF_u and LF_d. For example, LF_1 increases by 11% and 22% for Case 1 and Case 2, respectively, compared to that of the base case. For these same cases, LF_u increases by 6% and 13% respectively; for changes in positive bending capacities, LF_d increases by the same percentages 6% and 13%. The redundancy ratio for the ultimate condition, R_u and R_d decrease by 4% and 7% for Case 1 and Case 2, respectively.

Although all the load factors, LF_1, LF_u and LF_d in Case 3 and Case 4 decrease, the redundancy ratios increase. Weaker bridge girders lead to larger redundancy ratios. When the member capacities are reduced by 25% and 50% for Case 3 and Case 4, the redundancy ratio for the ultimate limit state, R_u increases by 15% and 37% respectively and the redundancy ratio for the damage condition, R_d increases by 14% and 46% for Case 3 and Case 4, respectively. These results are plotted in Figure 3.6 which shows similar trends as those of Figure 3.4. However, the effect of the change in the positive capacity is more significant than changes in both the positive and negative capacities. .

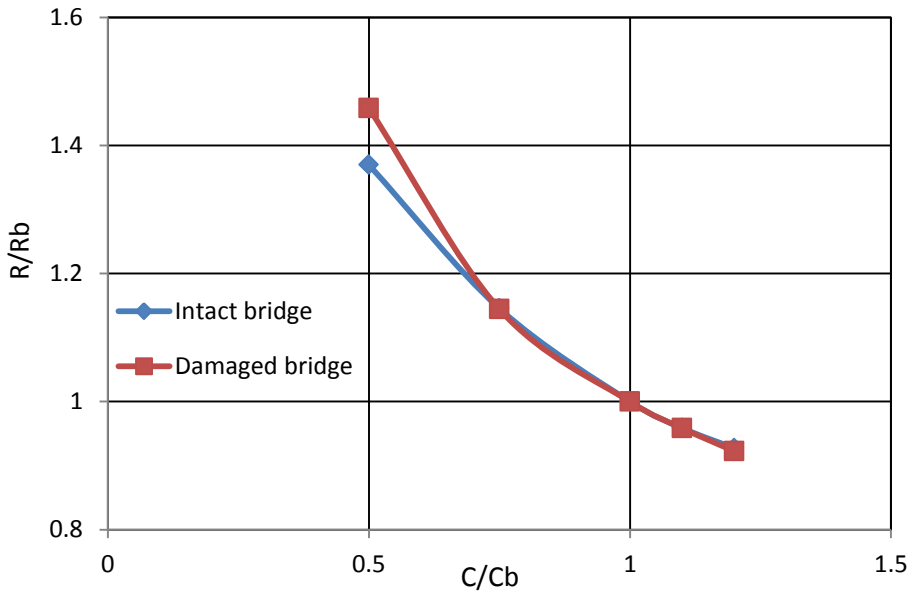

Figure 3.6 Effect of positive capacity ratio on redundancy ratio results

3) Only negative bending moment is changed.

Four cases are analyzed to investigate the effect of changes in the negative bending moment capacity as listed below:

Case 1: Change negative moment capacity only by+10%,
Case 2: Change negative moment capacity only by+20%,
Case 3: Change negative moment capacity only by -25%,
Case 4: Change negative moment capacity only by-50%,

The load deflection curves for the Base case and Cases 1 through 4 are shown in Figure 3.7. The redundancy ratios are summarized in Table 3.3. The effect of member capacity changes on the redundancy ratio are plotted in Figure 3.8.

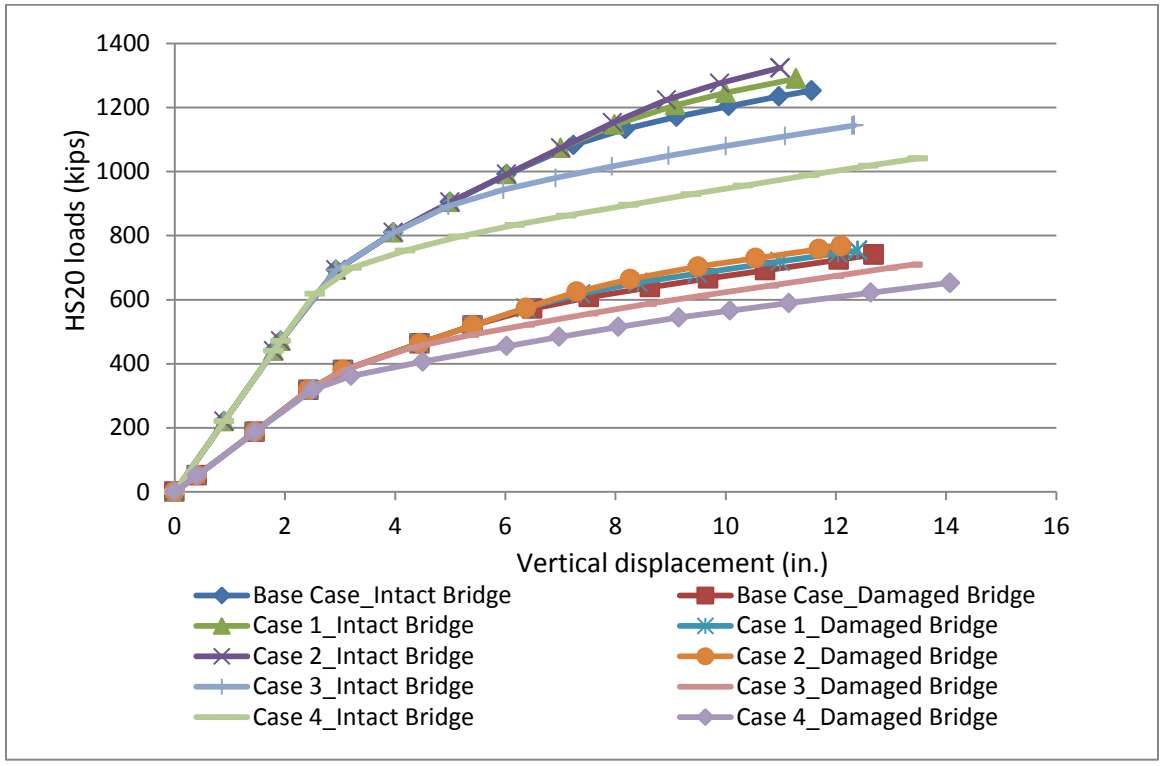

Figure 3.7 Load deflection curves for different negative member resistances

Table 3.3 Comparison of results of redundancy analysis for various changes in negative member resistance

3-span bridge	LF_1*	LF_{300}	LF_{200}	LF_{100}	LF_u	LF_d	R_{f100}	R_u	R_d
Base case	6.96	5.02	6.15	8.25	8.70	5.14	1.18	1.25	0.74
Case 1	6.96	5.02	6.15	8.53	8.96	5.23	1.23	1.29	0.75
Case 2	6.96	5.02	6.15	8.75	9.19	5.33	1.26	1.32	0.77
Case 3	6.96	5.02	6.10	7.42	7.95	4.92	1.07	1.14	0.71
Case 4	6.61	4.84	5.42	5.55	7.23	4.53	0.84	1.09	0.69

Note: * The value of LF_1 is the minimum load factor of positive bending moment and negative bending moment failure. Case 4 was governed by negative bending; other cases were governed by positive bending.

From Table 3.3, it is observed that the load factors, LF_1 remain constant except for Case 4 because the positive moment controls the first member failure in Cases 1 through 3 while Case 4 is governed by the negative bending moment In all the cases the load factors, LF_u and LF_d increase as the negative moment capacity increases and vice versa. Therefore, the redundancy ratios increase as the negative resistance capacity increases. In other words, stronger negative resistance capacity means larger redundancy ratios.

When the negative bending capacities are increased by 10% and 20% for Case 1 and Case 2, the redundancy ratio for the ultimate limit state, R_u increases 3% and 6%. The redundancy ratio for the damage condition, R_d increases 2% and 4% respectively.

When the negative capacities are reduced by 25% and 50% for Case 3 and Case 4, the redundancy ratio for the ultimate limit state, R_u reduces by 9% and 12%, while the redundancy ratio for the damage condition, R_d reduces by 4% and 7% as plotted in Figure 3.8. Overall, the negative capacity has a minor effect on the redundancy ratios of this particular three-span continuous bridge. Also, the relationship between the negative capacity and redundancy ratios may be taken as linear.

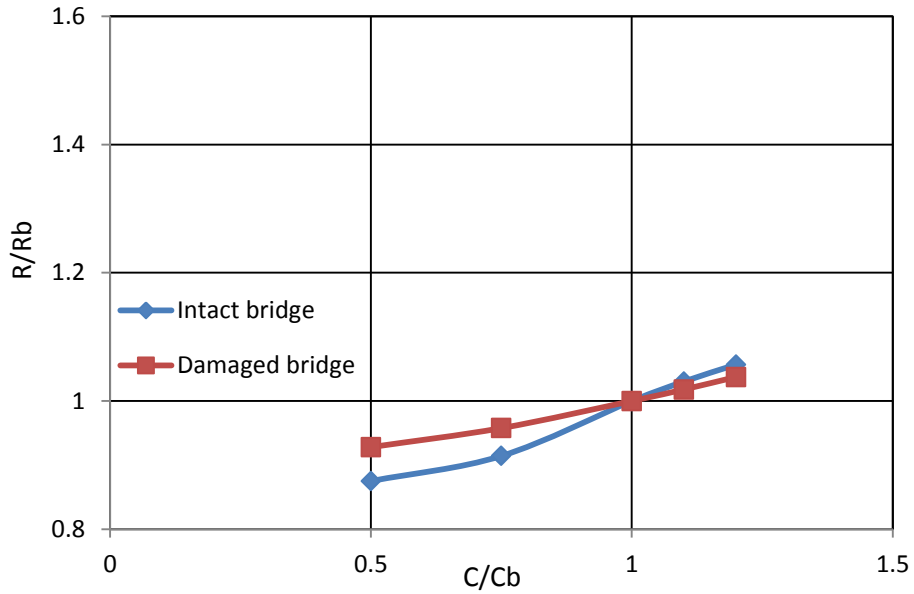

Figure 3.8 Effect of negative capacity ratio on redundancy ratio results

4) Steel girder section is changed

In the base bridge case, the positive bending segment was a formed by a W 36×170 steel section acting compositely with the deck and a W 36×160 steel I-girder is used in the negative moment regions. The analyses performed above assumed that the Moment-curvature plot is shifted upward by a certain percentage without changing the curvature. In this paragraph we investigate whether the observations made earlier are still valid when more realistic moment-curvature relationships are used. Therefore, the steel I-girders for both the positive and negative regions are changed to W 30×148 and the analysis is performed with the corresponding moment-curvature relationships. The following three cases are analyzed:

Base case: Positive region: W 36×170; Negative region: W 36×160;

Case 1: Only plastic hinge properties at positive and negative moment regions changed, elastic cross section properties are kept as those of the Base case;

Case 2: Both of plastic hinge properties and cross section properties are changed.

Case 1 is considered to study the effect of changes in the elastic properties on the final results. Moment curvature curves valid for both Cases 1 & 2 are compared to those of the base case for positive bending regions and negative bending regions in Figure 3.9 and Figure 3.10, respectively. The load deflection curves for the Base case and Cases 1 and 2 are shown in Figure 3.11. The cross section properties of the sections in the positive moment region and negative regions are listed in Table 3.4 and 3.5, respectively. The redundancy ratios are summarized in Table 3.6.

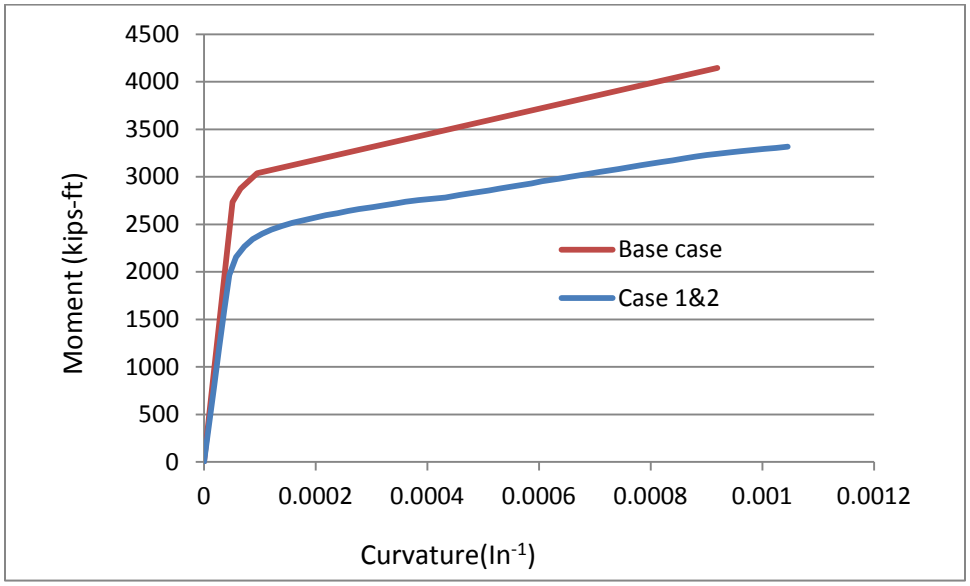

Figure 3.9 M-phi curves for composite steel I girders for the Base case and Case 1 & 2 for positive moment

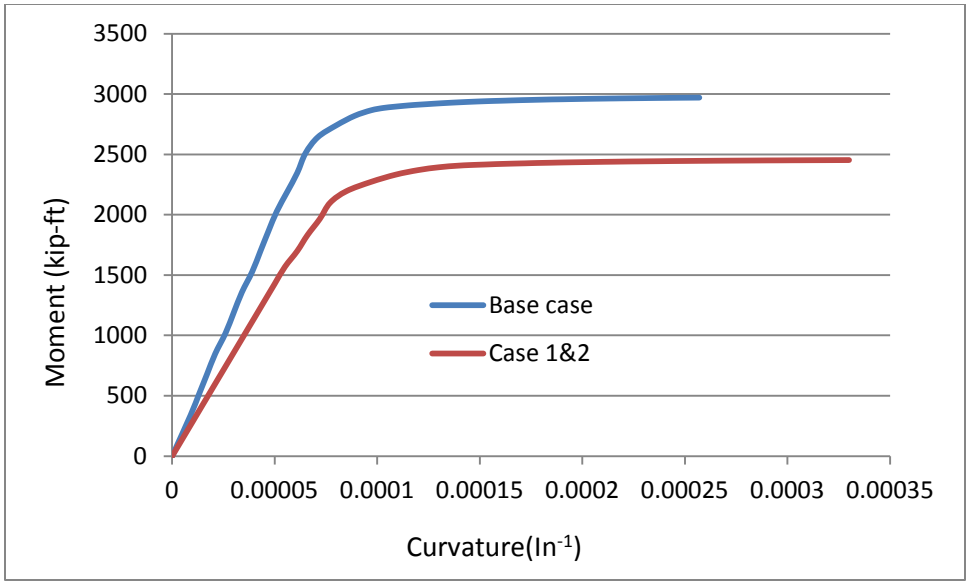

Figure 3.10 M-phi curves for composite steel I girders for the Base case and Case 1 & 2 for negative moment

Table 3.4 Gross superstructure properties for positive moment region_ based on steel girder material

3-span bridge	A (ft^2)	I_{xx} (ft^4)	I_{yy} (ft^4)	Weight (pcf)
Base case	1.107	1.30	4.07	786
Case 1	1.107	1.30	4.07	786
Case 2	1.062	0.88	4.06	798

Table 3.5 Effective* superstructure properties for negative moment region _ based on steel girder material

3-span bridge	A (ft^2)	I_{xx} (ft^4)	I_{yy} (ft^4)	Weight (pcf)
Base case	0.338	0.50	0.01	505
Case 1	0.338	0.50	0.01	505
Case 2	0.314	0.34	0.01	506

***Contribution of concrete slab at negative moment region is not taken into consideration.

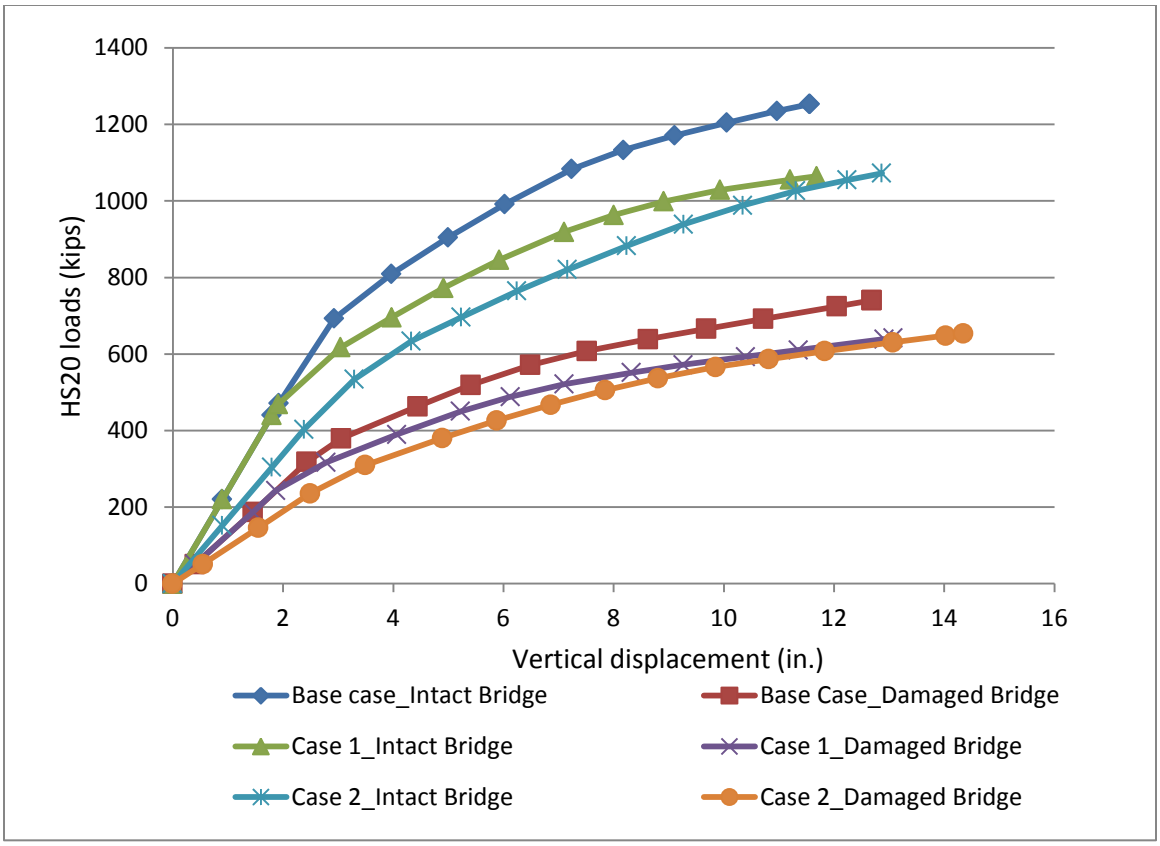

Figure 3.11 Load- deflection curves for different girder sections

Figure 3.11 compares the load versus maximum deflection curve for the base case and those of Cases 1 & 2. The ultimate capacities for the base case, Case 1 and Case 2 are 1,252.9 kips, 1,064.4 kips and 1,072.3 kips, respectively. Also, the ultimate capacities are 740.6 kips, 641.8 kips and 653.7 kips for the damaged bridge. The similarities of the results for Cases 1 and 2 demonstrate that the effect of the member stiffness is not significant although the overall load response curve is softer for the case where the elastic section properties are reduced.

Because of the smaller steel girder for the composite girder section in Cases 1 & 2, the three-span continuous bridge has an ultimate girder capacity equal to $R=M_p=39{,}788$ Kip-in. This is compared to $M_p=49{,}730$ kip-in for the base case. Using the linear elastic analysis, the moment for Case 2 due to the dead load at the mid-span of a girder is slightly lower than that of the Base case and Case 1 (D=4,860 kip-in) and is calculated to be D=4,730 kip-in. The external girder for Case 2 will carry a linear elastic moment equal to 6,366 kip-in due to the two side-by-side AASHTO HS-20 vehicles, while for the Base case and Case 1, the values are 6,450 kip-in.

Therefore, the load factors for first member failure of Case 1 and Case 2 are found to be LF_1=5.42 and LF_1=5.51, respectively, as seen in Table 3.6. A slightly higher LF_1 is obtained for the section with the lower stiffness because a bridge with beams with lower stiffness will distribute a higher portion of the applied live load to the beams farther away from the load when performing a linear elastic analysis.

Table 3.6 Comparison of results of redundancy analysis of various sections

3-span bridge	LF_1	LF_{300}	LF_{200}	LF_{100}	LF_u	LF_d	R_{f100}	R_u	R_d
Base case	6.96	5.02	6.15	8.25	8.70	5.14	1.18	1.25	0.74
Case 1	5.42	4.38	5.30	7.08	7.39	4.46	1.31	1.36	0.82
Case 2	5.51	3.61	4.63	6.62	7.45	4.54	1.20	1.35	0.82

From Table 3.6, it is observed that LF_1 decreases significantly for Cases 1 and 2 as compared to the base case. The reason is that smaller steel girders are used for Case 1 and 2, which leads to lower bending moment capacities, as seen in Figure 3.9 and 3.10.

Although the load factors, LF_1, LF_u and LF_d in Case 1 and Case 2 decrease, the redundancy ratios increase. Weaker steel girders for the composite beam lead to larger redundancy ratios. Positive bending moment capacities are reduced by 20% for Cases 1 and 2. At the same time, the redundancy ratios increase by 8.8% and 10.8% for the ultimate limit state and the damage condition, respectively. These changes are slightly higher than those observed when the Note that R_u and R_d are essentially the same for Cases 1 and 2 demonstrating the lack of sensitivity of these results to changes in the stiff nesses of the beams even though the load factors, LF_{300}, LF_{200} and LF_{100} for Case 2 are smaller than those of Case 1.

From the above discussion on the effect of changes in the beam resistance on the 3-span continuous bridge, the following conclusions can be drawn:

(1) Variation of the redundancy ratio R_u is roughly on the order of 8% when the girder capacity (both of positive and negative moment) changes by less than 20%.
(2) The redundancy ratio R_d, changes by about 10% for a 20% change in member capacity.
(3) The changes in the redundancy ratio are in the opposite sense of the change in the moment capacity such that a decrease in member capacity leads to an increase in the redundancy ratio.
(4) This effect is most significant for changes in the positive moment capacity.

3.1.2 Simple span bridges

In this section we analyze the effect of resistance over dead R/D ratio for simply supported bridges. The span length is increased from 80-ft to 100-ft. The simple bridges have four beams with 8-ft spacing. For the base case scenario, the moment capacity of each beam is assumed to meet the design criteria of the AASHTO LFD Design Code. Accordingly, the external girder at mid-span will carry a linear elastic positive moment equal to 9,193 kip-in and 11,811 kip-in for 80-ft span bridge and 100-ft span bridge, respectively, due to side-by-side AASHTO HS-20 trucks. The results of the analysis for the ultimate limit state are summarized in Table 3.7. Several cases are analyzed consisting of changing the dead load moment by +/- 40%, the moment capacity by +/- 40% for each of the 80-ft simple span and 100-ft simple span bridges. The results show insignificant results in the redundancy ratio for the ultimate limit state, R_u which varies between a maximum value of R_u=1.25 and a minimum value of R_u=1.13 even though LF_1 and LF_u change by up to 50%. This observation confirms that the redundancy ratio R_u is not sensitive to changes in the member capacities or the dead load intensities for simple span bridges. However, heavy dead load is to produce a lower redundancy ratio R_d. R_d varies between a maximum value of R_d=0.65 and a minimum value of R_d=0.44.

Table 3.7 Summary of results for simple span bridges with different R and D values

Simple Span Length	R (ft-in)	D (ft-in)	R/d	LF_1	LF_u	R_u	R_d**
Design*	45039	9326	4.83	3.66	4.70	1.19	0.60
80ft	45039(--)	10259(+10%)	4.39	3.57	4.58	1.19	0.59
80ft	45039(--)	11191(+20%)	4.02	3.47	4.46	1.19	0.58
80ft	45039(--)	13056(+40%)	3.45	3.28	4.20	1.20	0.55
80ft	45039(--)	8393(-10%)	5.37	3.76	4.83	1.19	0.60
80ft	45039(--)	7461(-20%)	6.04	3.86	4.95	1.18	0.61
80ft	45039(--)	5596(-40%)	8.05	4.05	5.19	1.17	0.63
80ft	49543(+10%)	9326(--)	5.31	4.13	5.26	1.18	0.59
80ft	54047(+20%)	9326(--)	5.80	4.59	5.83	1.16	0.59
80ft	63055(+40%)	9326(--)	6.76	5.51	6.91	1.14	0.59
80ft	40535(-10%)	9326(--)	4.35	3.20	4.12	1.21	0.60
80ft	36031(-20%)	9326(--)	3.86	2.74	3.55	1.22	0.60
80ft	27023(-40%)	9326(--)	2.90	1.82	2.37	1.24	0.62
80ft	49730(+10%)	8393(-10%)	5.90	4.24	5.40	1.17	0.60
80ft	54047(+20%)	7461(-20%)	7.24	4.78	6.06	1.15	0.60
80ft	63055(+40%)	5596(-40%)	11.27	5.90	7.36	1.13	0.61
Design*	63429	14966	4.24	3.81	4.89	1.25	0.62
100ft	63429	16463(+10%)	3.85	3.69	4.736	1.21	0.59
100ft	63429	17959(+20%)	3.53	3.57	4.58	1.21	0.62
100ft	63429	20952(+40%)	3.03	3.34	4.29	1.16	0.44
100ft	63429	13469(-10%)	4.71	3.92	5.03	1.21	0.63
100ft	63429	11973(-20%)	5.30	4.04	5.20	1.21	0.60
100ft	63429	8980(-40%)	7.06	4.28	5.50	1.20	0.65
100ft	69772(+10%)	14966	4.66	4.31	5.51	1.20	0.60
100ft	76115(+20%)	14966	5.09	4.80	6.12	1.19	0.61
100ft	88801(+40%)	14966	5.93	5.80	7.32	1.15	0.60
100ft	57086(-10%)	14966	3.81	3.31	4.27	1.22	0.62
100ft	50743(-20%)	14966	3.39	2.81	3.64	1.22	0.61
100ft	38057(-40%)	14966	2.54	1.81	2.36	1.25	0.61
100ft	69772 (+10%)	13469 (-10%)	5.18	4.42	5.67	1.20	0.62
100ft	76115 (+20%)	11973 (-20%)	6.36	5.04	6.42	1.18	0.63
100ft	88801 (+40%)	8980 (-40%)	9.89	6.27	7.87	1.14	0.63

Note: *The moment capacity is designed by AASHTO LRFD Code.

** Weight of the damaged beam is included and transferred to the adjacent beam.

3.2 Effect of plastic hinge length

In the base bridge case, we are using plastic hinge length, L_p=d/2, where d is the depth of bridge girders. Because there are many different models and different researchers have used different

approaches for determining the plastic hinge length, a sensitivity analysis is performed to study the effect of this parameter on the results. In this section we compare the results obtained in the base case with L_p=d/2 to those when the plastic hinge is assumed to be L_p=0.75 d, 1.0d and 1.50 d. For the Base case, L_p=25.1 in. is used for the plastic hinge in the positive moment region and L_p=18.5 in is used in the negative moment region. Three additional cases are analyzed to investigate the effect of plastic hinge length as follows:

Case 1: L_p=0.75d: positive bending L_p=37.65 in., negative bending L_p=27.75 in.
Case 2: L_p=1.00d: positive bending L_p=50.20 in., negative bending L_p=37.00 in.
Case 3: L_p=1.50d: positive bending L_p=75.30 in., negative bending L_p=55.50 in.

The load deflection curves for the Base case and Cases 1, 2 and 3 are shown in Figure 3.12. The plots in the figure demonstrate that the load response curves remain practically the same showing as expected a slightly more flexible behavior as L_p increases. Although the failure point occurs earlier for the smaller plastic hinge lengths, this does not affect the prediction of the ultimate capacity significantly because the slope of the load response curve is small at high loads. The redundancy ratios are summarized in Table 3.8. The variations of the redundancy ratios for the ultimate limit state (R_u) and the damage limit state (R_d) versus L_p/d are illustrated in Figure 3.13. The results show a maximum difference of about 5% for R_u and 10% for R_d. Therefore, it is concluded that the plastic length has only a minor effect on the redundancy ratios.

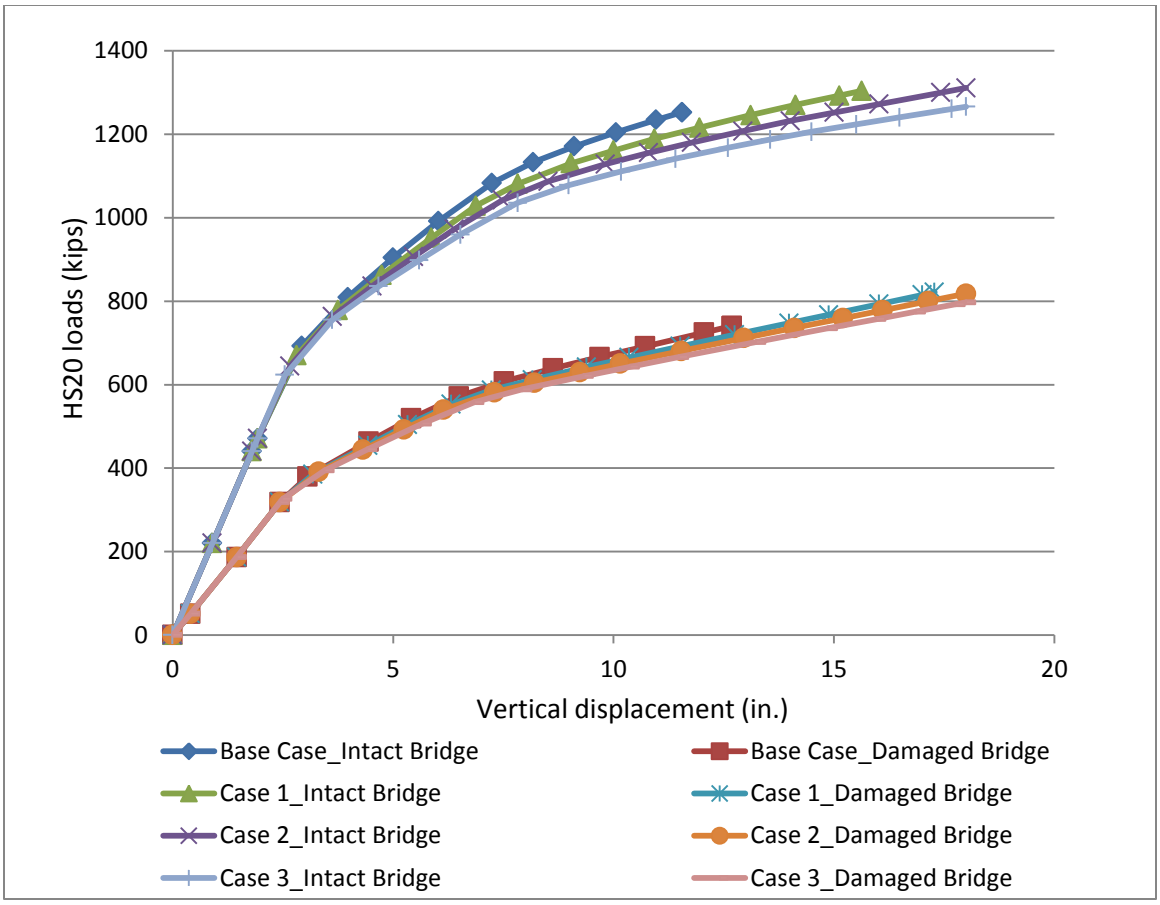

Figure 3.12 Load deflection curves for the Base case different plastic hinge length

Table 3.8 Comparison of results of redundancy analysis for different plastic hinge length

3-span bridge	LF_1	LF_{300}	LF_{200}	LF_{100}	LF_u	LF_d	R_{f100}	R_u	R_d
Base case	6.96	5.02	6.15	8.25	8.70	5.14	1.18	1.25	0.74
Case 1	6.96	4.97	6.03	7.97	9.06	5.70	1.15	1.30	0.82
Case 2	6.96	4.93	5.95	7.79	9.10	5.68	1.12	1.31	0.82
Case 3	6.96	4.89	5.86	7.61	8.79	5.54	1.09	1.26	0.80

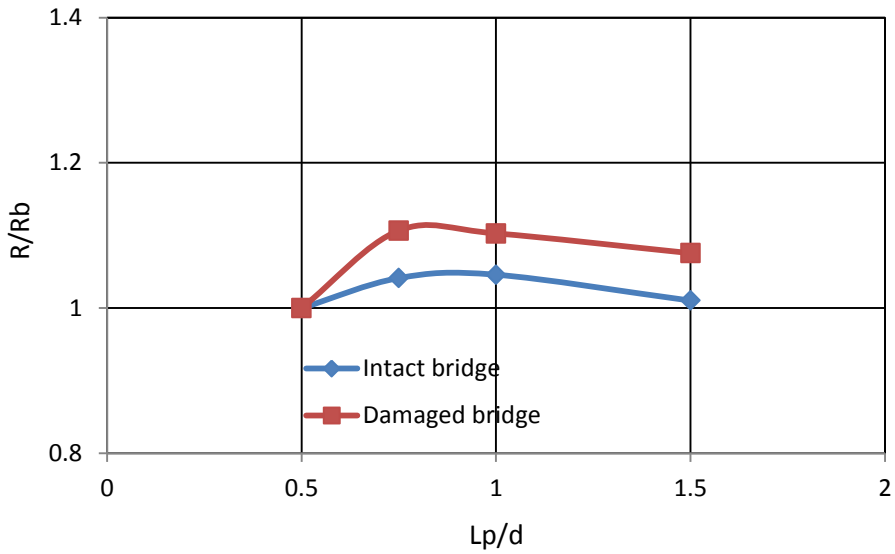

Figure 3.13 Effect of plastic length ratio on redundancy ratio results

3.3 Effect of truck placement

Two cases are analyzed to investigate the effect of truck placement compared to the base case as follows:

Base case: Two side by side trucks in the middle span;
Case 1: Two side by side trucks in each of two spans;
Case 2: One truck in each of two spans.

The Influence line for the negative bending moment at the interior support is shown in Figure 3.14. To produce the highest negative moment, the middle axles of the HS-20 trucks are placed at the sections having the largest negative influence value in each span as depicted in Figure 3.14. This loading scenario is selected to investigate the redundancy of the system if failure is initiated in the negative bending region.

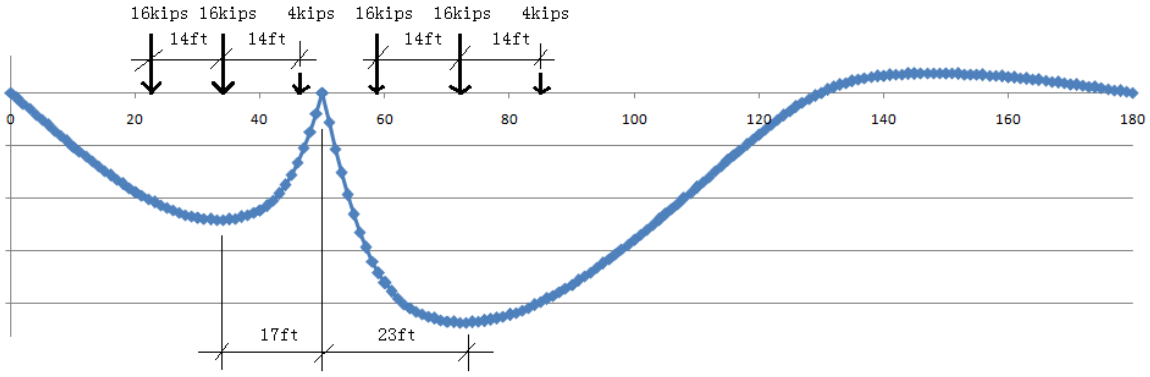

Figure 3.14 Influence line for negative bending moment

Case 1: The negative moment capacity at the section over the interior support is R= M^- = 46,188 Kip-in (3,849 kip-ft). For Case 1, the negative moment due to the dead load at the interior support of a girder is obtained as D=2,799 kip-in. The external girder section over the interior support will carry a linear elastic negative moment equal to 4,361 kip-in due to four AASHTO HS-20 trucks with two trucks in each loaded span. Therefore, the load factor for first member failure in negative bending is LF_1=9.95.

Case 2: The negative moment due to the dead load at the interior support of a girder is obtained as D=2,799 kip-in. The external girder section over the interior support will carry a linear elastic negative moment equal to 3,572 kip-in due to two AASHTO HS-20 trucks with one truck in each loaded span. Therefore, the load factor for first member failure in negative bending is LF_1=12.15.

The load displacement curves for the base case and Cases 1 and2 are shown in Figure 3.15. The results show that LF_u, LF_f, LF_d and LF_1 will change significantly as summarized in Table 3.9.

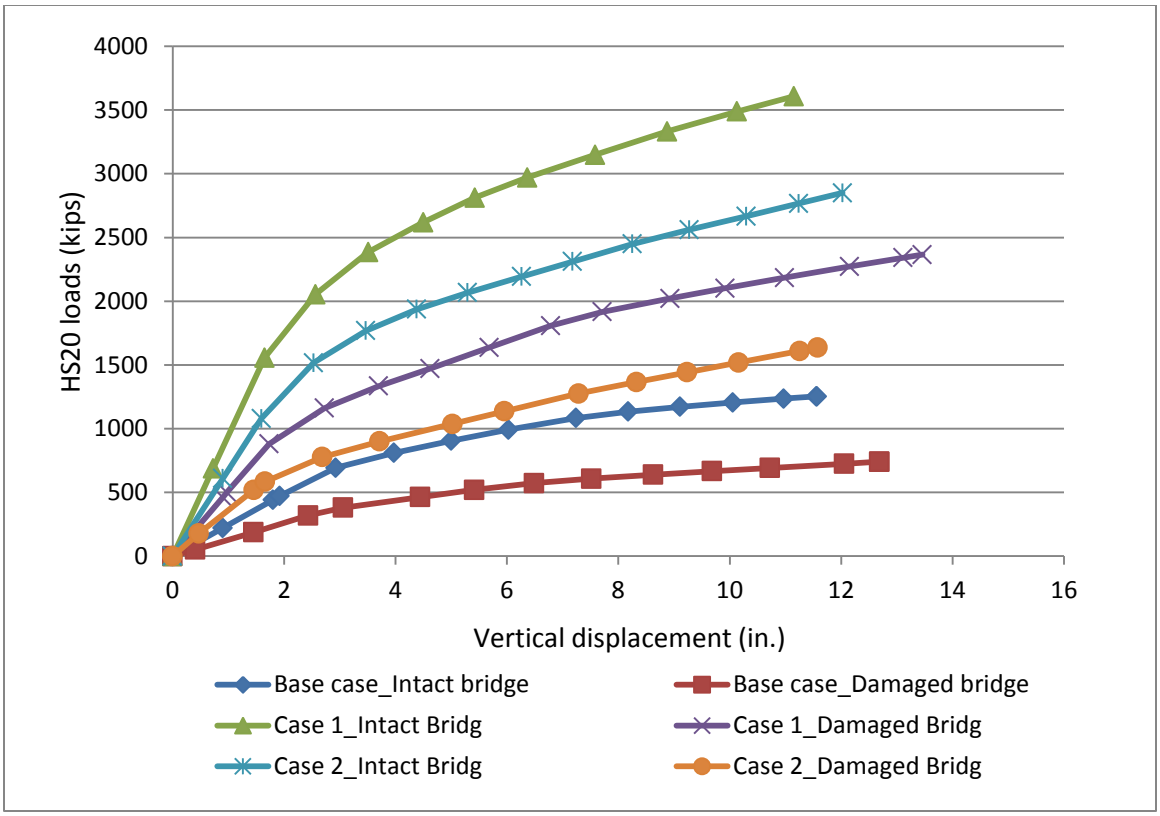

Figure 3.15 Figure 1.15 Load deflection curves for different truck loading scenarios

Table 3.9 Comparison of results of redundancy analysis of positive and negative moment failure

3-span bridge	LF_1	LF_{300}	LF_{200}	LF_{100}	LF_u	LF_d	R_{f100}	R_u	R_d
Base case	6.96	5.02	6.15	8.25	8.70	5.14	1.18	1.25	0.74
Case 1	9.95*	7.90	9.31	11.88	12.52	8.21	1.19*	1.26*	0.83*
Case 2	12.15	11.78	13.87	18.02	19.79	11.36	1.48	1.63	0.93

Note: * These values are modified as compared to last quarterly report. The negative moment capacity at the section over the interior support should be R= M^- = 46,188 Kip-in (3,849 kip-ft).

From Table 3.9, it can be observed that all the load factors including LF_1, LF_f, LF_u, LF_d as well as the redundancy ratios increase when the initiation of failure is in the negative bending region, especially for Case 2. It can be concluded that for this three-span bridge configuration, the members in the positive bending region control the redundancy ratios. This observation along with the low probability of having four excessively heavy trucks simultaneously on the bridge in the worst position indicate that the Base case loading of side-by-side trucks in a single span is more likely to control the redundancy of multi-span bridges.

3.4 Effect of span length configuration of 3-span continuous bridges

In the base bridge case, the three span lengths are 50ft-80ft-50ft. In this section we analyze the effect of changing the spans' lengths and two additional cases are considered. In Case 1, the span length configuration is changed to 75ft-100ft-75ft and in Case 2 we use a bridge with three spans of 110ft-150ft-110ft. The analysis is performed assuming that the member capacities remain the same. The load deflection curves for the Base case and Cases 1 & 2 are shown in Figure 3.16. The redundancy ratios are summarized in Table 3.10 which shows significant increases in the redundancy ratios as the span lengths increased even though the load factor for first member failure LF_1 and for the system intact and damaged systems LF_u and LF_d decrease.

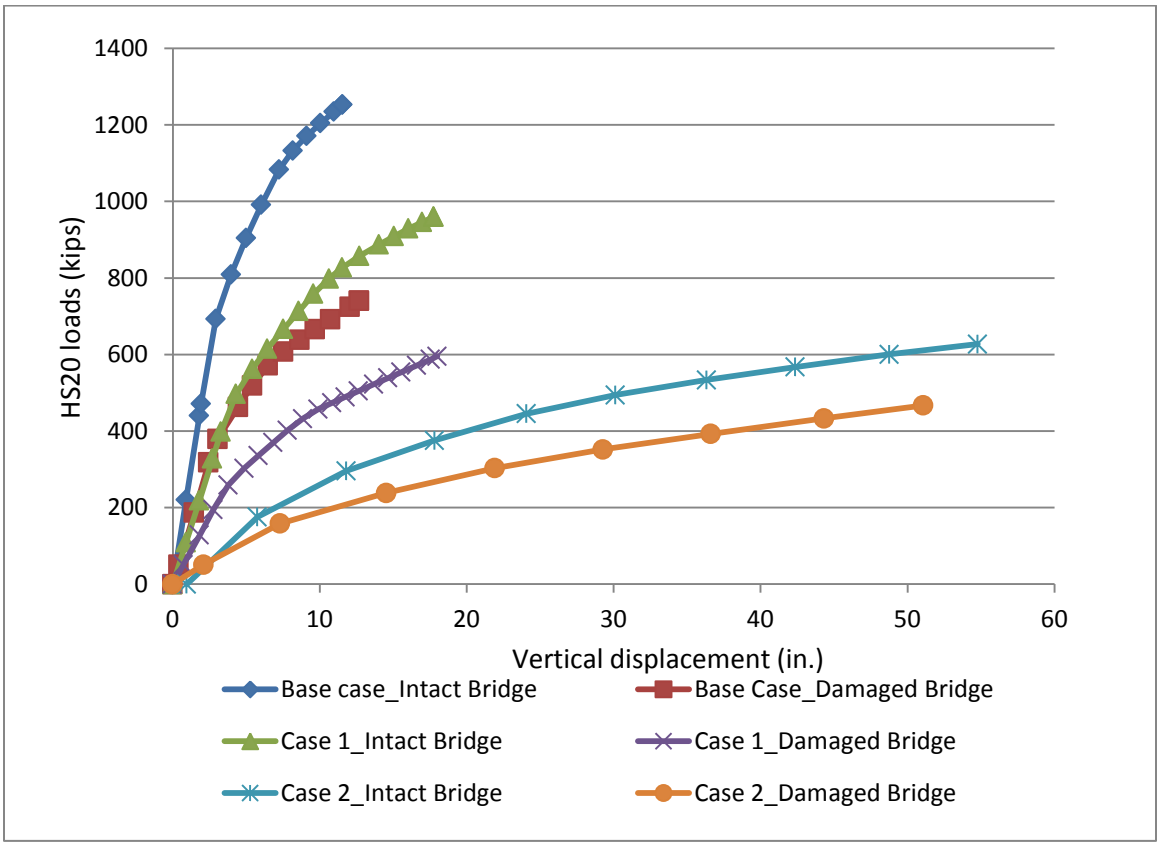

Figure 3.16 Load deflection curves for different span configuration

Figure 3.16 compares the load versus maximum deflection curve for the base case and Case 1 & 2 three-span continuous bridges. The ultimate capacities for the base case, Case 1 and Case 2 are 1,252.9 kips, 960.1 kips and 627.3 kips, respectively. Also, the ultimate capacities are 740.6 kips, 595.2 kips and 467.1 kips for the damaged bridge.

The composite girder section used for the Base case and Case 1 & 2 three-span continuous bridge has an ultimate girder capacity equal to $R=M_p=39{,}788$ Kip-in. Using the linear elastic analysis, the moments due to the dead load at the mid-span of a girder for Case 1 and Case 2 are calculated to be D=7,984 kip-in and D=16,868 kip-in. The external girder for Case 1 will carry a linear elastic moment equal to 8,561 kip-in due to the two side-by-side AASHTO HS-20 vehicles, while for Case 2, the values are 13,068 kip-in. Therefore, the load factors for first member failure of Case 1 and Case 2 are found to be $LF_1=3.71$ and $LF_1=1.75$, respectively, as seen in Table 3.10.

Table 3.10 Comparison of results of redundancy analysis of various span configurations

3-span bridge	LF_1	LF_{300}	LF_{200}	LF_{100}	LF_u	LF_d	R_{f100}	R_u	R_d
Base case	6.96	5.02	6.15	8.25	8.70	5.14	1.18	1.25	0.74
Case 1	3.71	2.70	3.69	5.28	6.67	4.13	1.42	1.80	1.11
Case 2	1.75	0.57	0.97	1.75	4.36	3.24	1.00	2.49	1.85

From Table 3.10, it is observed that LF_1 decreases significantly for Cases 1 & 2 as compared to the Base case. The reason is that for the longer span, the live load effect as well as the dead load effects are higher. Given the same member resistance a lower load factor will cause first member failure. This can also explain the changes of LF_u and LF_d.

It is obvious that the redundancy ratios, R_{f100}, R_u and R_d for Case 1 & 2 are much larger than those of the Base case. This is because the effect of the change in the ultimate capacity is less pronounced than that for first member failure. This trend follows the same trend observed earlier when the member resistances of the base three-span continuous bridge are changed.

3.5 Effect of bracing

The composite steel beam deck in the above sections has been analyzed without consideration of transverse bracing. In steel bridges, bracings are commonly placed between longitudinal beams primarily to distribute construction loads before the deck is poured and lateral loads from wind. Some engineers believe that bracing can also help distribute vertical traffic loads. Figure 3.17 shows some typical arrangements of bracing systems. Some bridge engineers do not take account of bracing in the grillage analysis for simplicity and on the assumption that it is conservative. Others include the bracing in the grillage model in order to check its loading and fatigue.

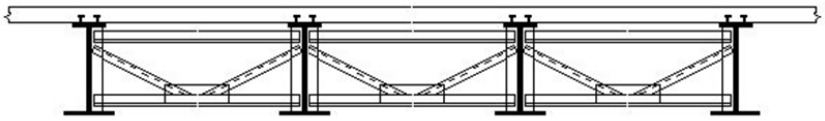

(a) K-bracing

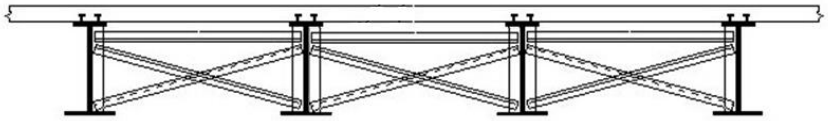

(b) X-bracing

(c) Braced abutment trimmer

Figure 3.17 Commonly used bridge bracing systems

Hambly (1991) observed that if plane frame analyses are carried out of single frames of K-bracing subjected to forces from the slab, the bracing provides relatively little additional stiffness to the slab. Transverse bracing has no effect on the stiffness of the slab if the web stiffeners are purposely not attached to the top flanges.

To study the effect of the additional stiffness that may be provided by the bracing on the results of the push-down curves and redundancy ratios, an approximate method is used which consists of amplifying the bending stiffness of the slab by different factors varying between 5% and 15% as follows:

Base case: No additional stiffness provided by bracing;

Case 1: Bending stiffness of slab increased by + 5%;

Case 2: Bending stiffness of slab increased by + 10%;

Case 3: Bending stiffness of slab increased by + 15%;

The load deflection curves for the Base case and the other three cases are shown in Figure 3.18. The redundancy ratios are summarized in Table 3.11.

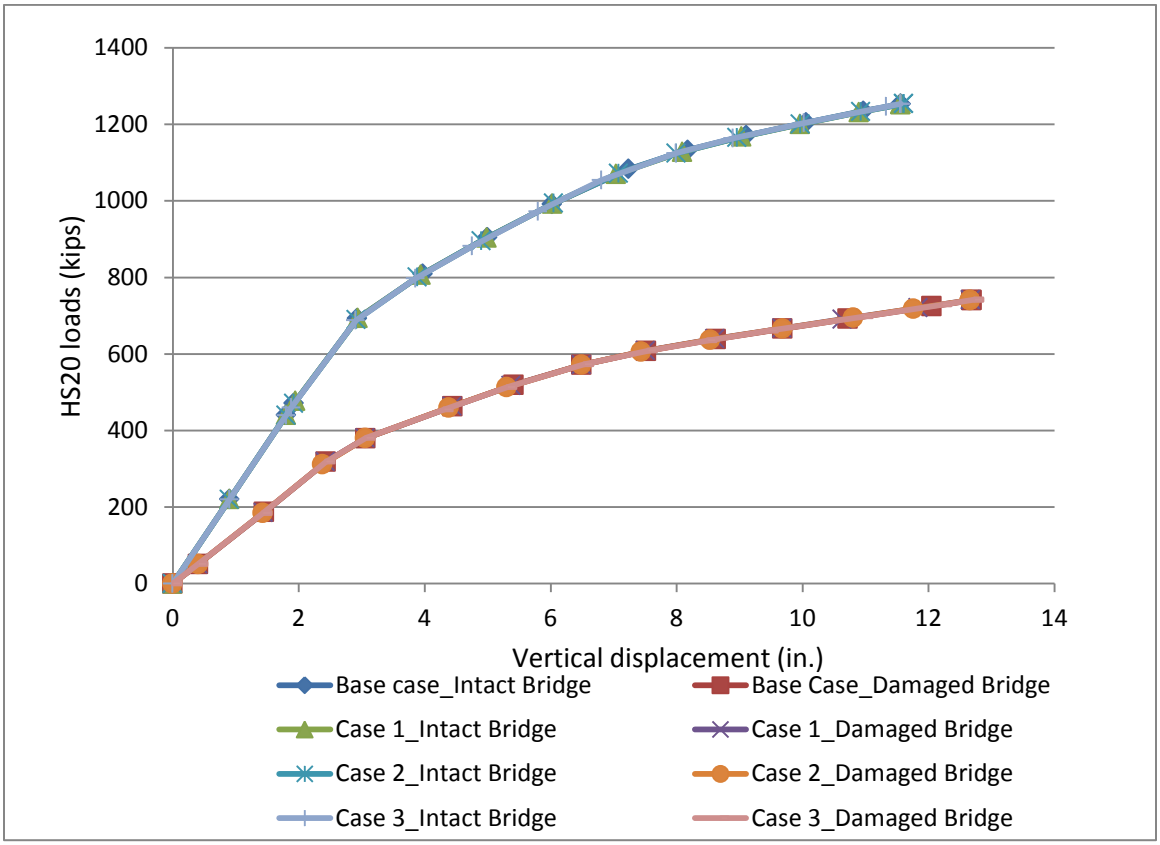

Figure 3.18 Load deflection curves for different bracing

Figure 3.18 compares the load versus maximum deflection curve for the base case and Case 1, 2 and 3 for the three-span continuous bridge. The results are essentially identical for all the cases considered for the whole range of performance including the linear elastic range and the load at failure for both the originally intact bridge and the damaged bridge with one member removed. It is therefore, concluded that bracing has no effect on the redundancy ratios.

Table 3.11 Comparison of results of redundancy analysis for different bracings

3-span bridge	LF_1	LF_{300}	LF_{200}	LF_{100}	LF_u	LF_d	R_{f100}	R_u	R_d
Base case	6.96	5.02	6.15	8.25	8.70	5.14	1.18	1.25	0.74
Case 1-3	6.96	5.02	6.15	8.25	8.70	5.14	1.18	1.25	0.74

3.6 Effect of the beam spacing

The results of NCHRP 406 have demonstrated that beam spacing has a major effect on bridge redundancy. In this section, two sets of analysis are performed. In the first set, we keep the same number of bridge beams and change the beam spacing. In the second set, the number of beams is changed but the bridge width is kept approximately the same by adjusting the number of beams.

3.6.1 Number of bridge beams unchanged

For the Base case, the six beams are at 8-ft spacing. Two additional cases are analyzed to investigate the effect of beam spacing as follows:

Base case: 8-ft. beam spacing;
Case 1: 6-ft. beam spacing;
Case 2: 10-ft. beam spacing.

Moment curvature curves for the beams used in the models of Cases1 and2 are compared to the base case. Variation of the beam spacing changes the moment-curvature relationship of the composite beams in positive bending as shown in Figure 3.19 because of the different effective widths of the concrete slab. The negative bending moment-curvature relationship is not affected. The load deflection curves for the Base case and Cases 1 and 2 are shown in Figure 3.20. The redundancy ratios are summarized in Table 3.12.

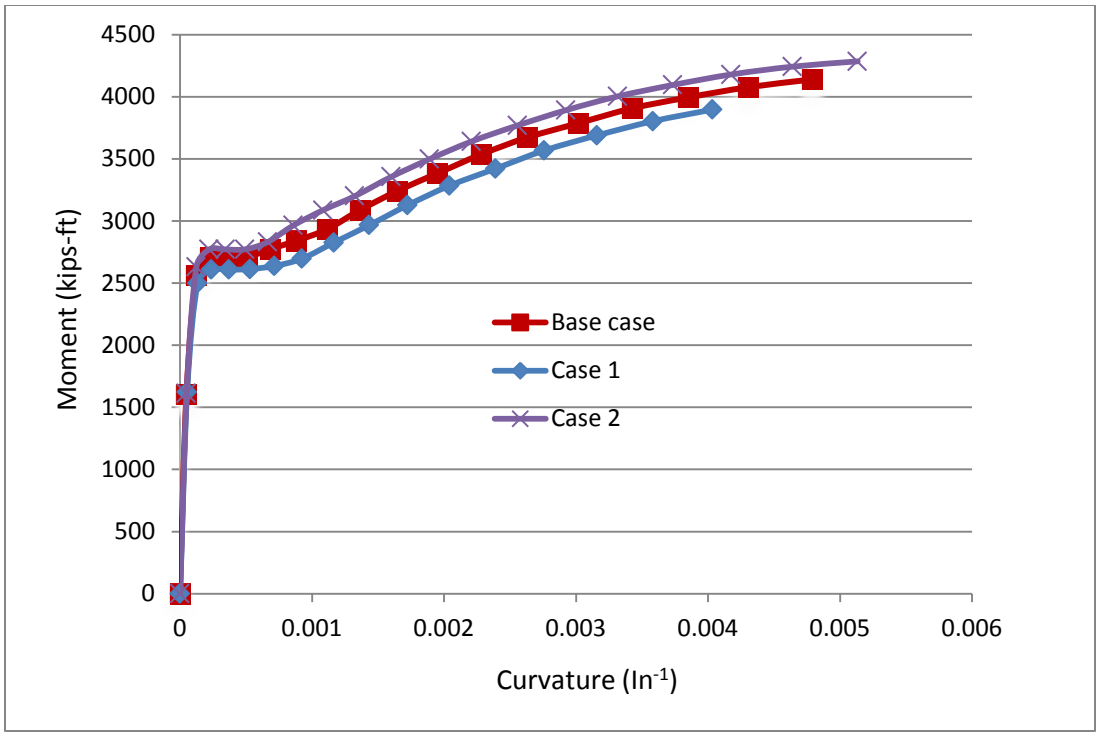

Figure 3.19 Moment-curvature relationship

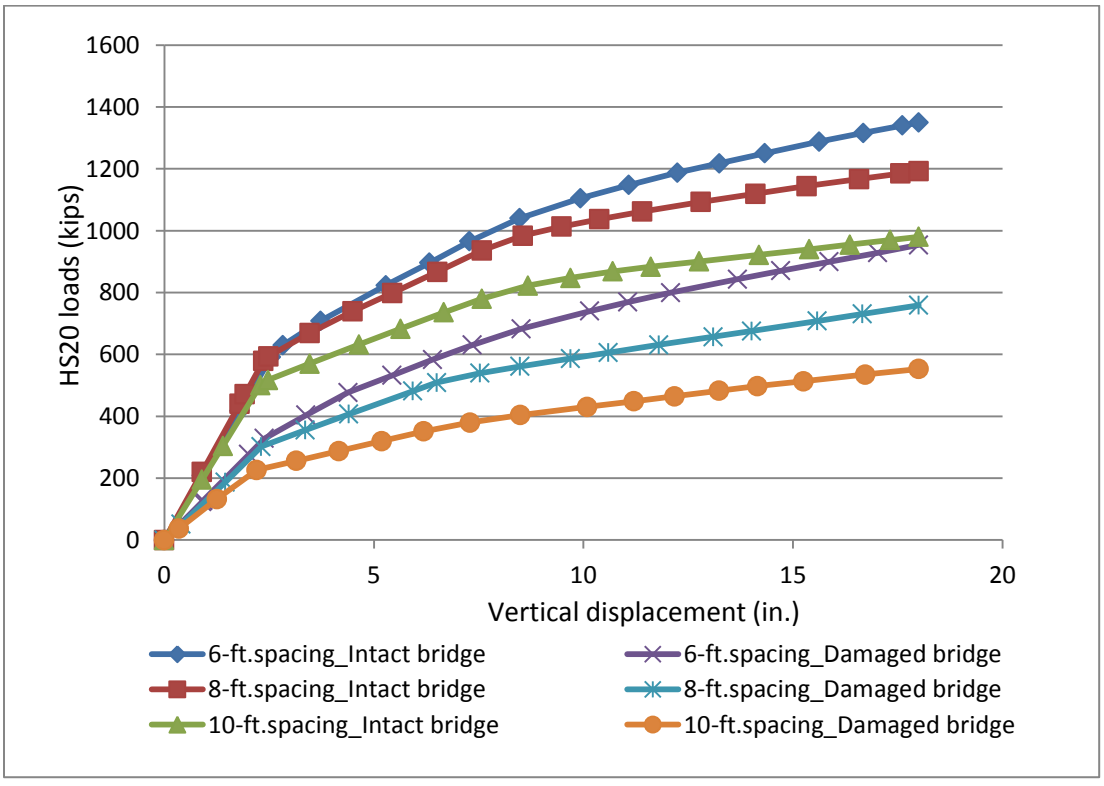

Figure 3.20 Load deflection curves for beam spacing 6-ft, 8-ft and 10-ft

The ultimate capacities for the Base case, Case 1 and Case 2 are found when the total applied live load is respectively equal to1,192.9 kips, 1,349.7 kips and 980.4 kips. The analysis of the damaged bridge scenario assumed two cases. For the damaged bridge scenarios when the external beam is removed from the model and the dead load of the removed beam is also removed, the ultimate capacities are reached when the applied live load reaches 759.0 kips, 953.7 kips and 553.0 kips. When the external beam is removed from the model but its dead load is not removed, the ultimate capacities are reached when the applied live load reaches 700.6 kips, 912.3 kips and 487.1 kips. The moment capacity of the beams at 6-ft spacing is R=46,758 kip-in, the dead load moment is D=3,840 kip-in, and the moment due to the AASHTO His S-20 truck LL=6,366 kip-in; For the beams at 8ft spacing, R=49,670 kip-in, D=4,860 kip-in, LL=6,450 kip-in; For the beams at 10ft spacing R=51,417 kip-in, D=5,488 kip-in, LL=7,466 kip-in; The corresponding load factors LF_1 for first member failure for the beams at 6ft, 8ft and 10ft spacing are found to be 6.74, 6.95 and 6.15 ,respectively, as summarized in Table 3.12. As expected, the results show that the effect of the beam spacing on the redundancy ratios is significant particularly for the damaged bridge scenario. If the damaged bridge has to also carry the weight of the damaged beam, the effect of the spacing is even more significant.

Table 3.12 Comparison of results of redundancy analysis of various resistance over dead load ratios

3-span bridge	LF_1	LF_u	LF_d	R_u	R_d*	R_d**
6ft (Case 1)	6.74	9.37	6.62	1.39	0.98	0.94
8ft (Base case)	6.95	8.28	5.27	1.20	0.76	0.70
10ft (Case 2)	6.15	6.81	3.84	1.11	0.62	0.55

Note: * Weight of damaged beams is not included in the damaged scenario.

** Weight of damaged beams is included and transferred to the remaining beams.

3.6.2 Bridge width kept constant

In this analysis set we assume that the effective width of the bridge remains practically the same at 48-ft so that when the beam spacing is changed, the number of beams is changed accordingly.

For the base case, we use 6 beams at 8-ft spacing. Case 1 consists of 8 beams at 6ft spacing; while Case 2 is for a bridge with 4 beams at 12-ft spacing.

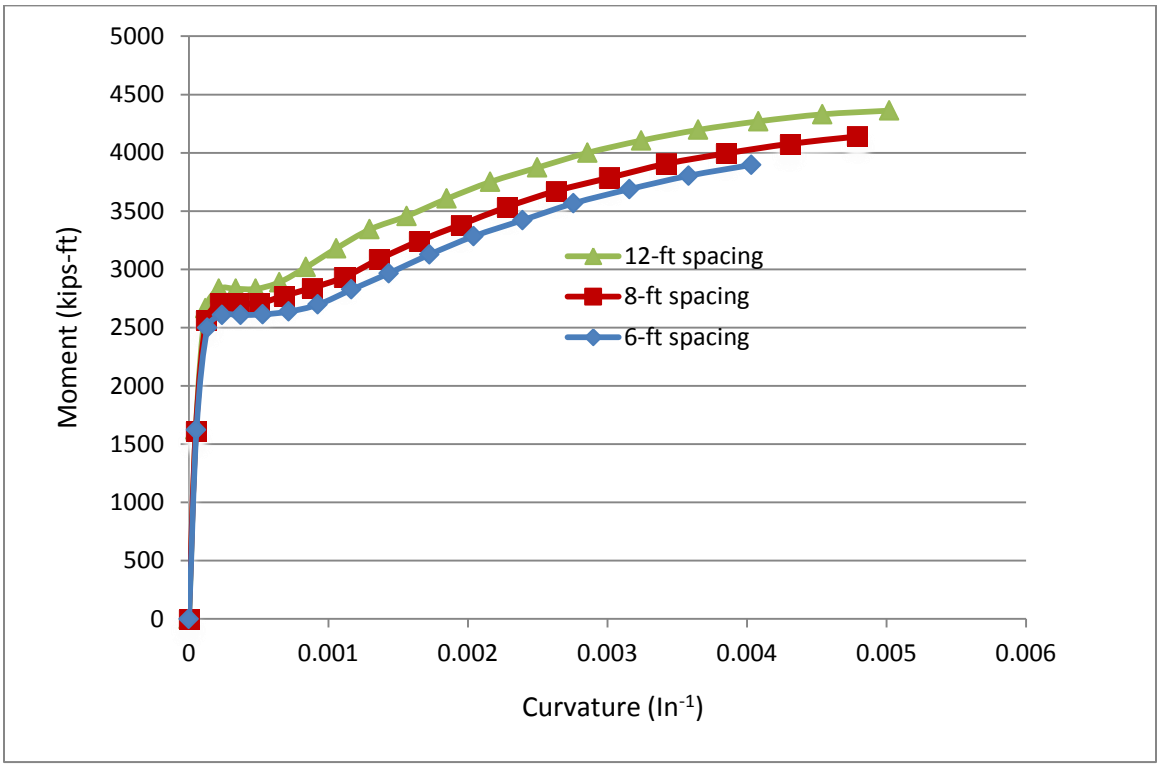

Figure 3.21 Moment-curvature relationship for beam spacing 12-ft, 8-ft and 6-ft

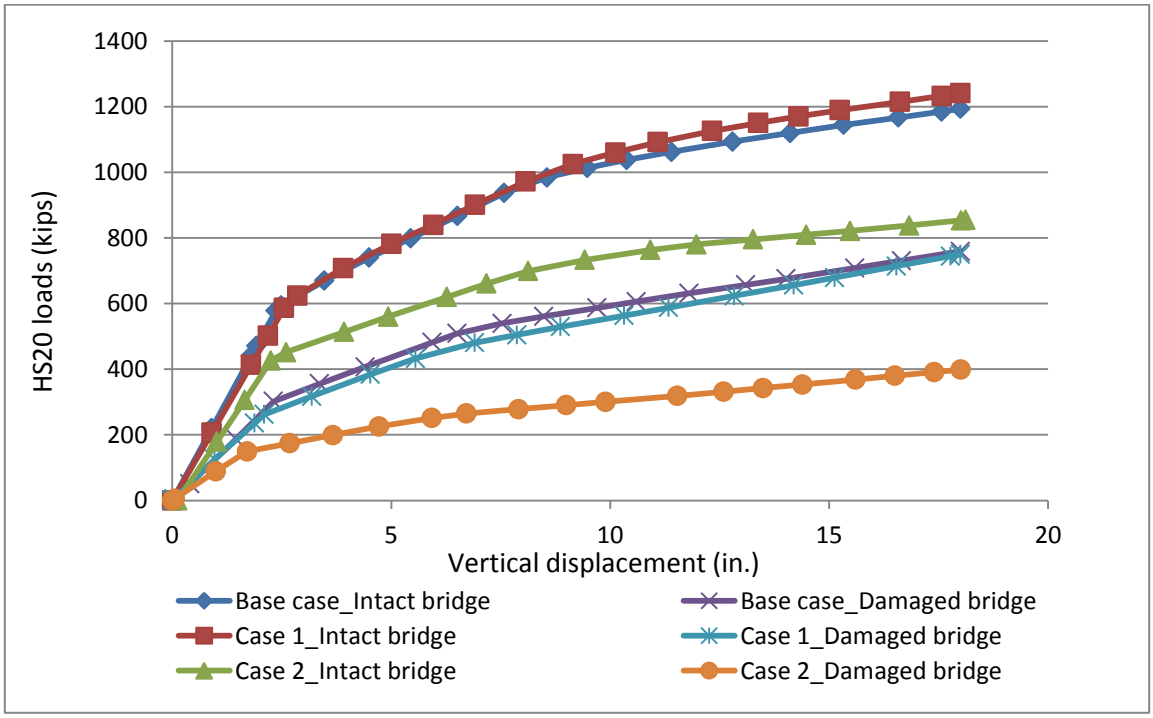

Figure 3.22 Load deflection curves for the Base case and Cases 1 & 2

Figure 3.22 compares the load versus maximum deflection curves for the three-span continuous bridge for the base case configuration and Cases 1 & 2. The ultimate capacities for the base case, Case 1 and Case 2 are 1,192.9 kips, 1,240.8 kips and 854.6 kips, respectively. Also, the ultimate capacities are 759.0 kips, 749.7 kips and 398.7 kips for the damaged bridge. The ultimate moment capacities of the beams, R, their dead loads, D, and the live load moment for the HS-20 truck, L, for cases 1 and 2 are given as:

Case 1 (6-ft spacing): R=46,758 kip-in, D=3,836 kip-in, LL=6,424 kip-in;

Case 2 (12-ft spacing): R=52,343 kip-in, D=6,884 kip-in, LL=8,399 kip-in;

The load factors and the redundancy ratios are summarized in Table 3.13. Figures 3.23 and 3.24 plot the redundancy ratios from Table 3.13 and 3.12 as a function of beam spacing. The plots demonstrate that the effect of the number of beams is not significant when the beam spacing is equal or larger than 8-ft. For spacing of 6-ft, increasing the number of beams will help improve the redundancy ratio.

Table 3.13 Comparison of results of redundancy analysis of various resistance over dead load ratios

3-span bridge	LF_1	LF_u	LF_d	R_u	R_d*
Base case	6.95	8.28	5.27	1.20	0.70
Case 1	6.68	8.62	5.21	1.29	0.78
Case 2	5.41	5.93	2.77	1.10	0.51

Note: * Weight of damaged beams is included and transferred to the adjacent beam.

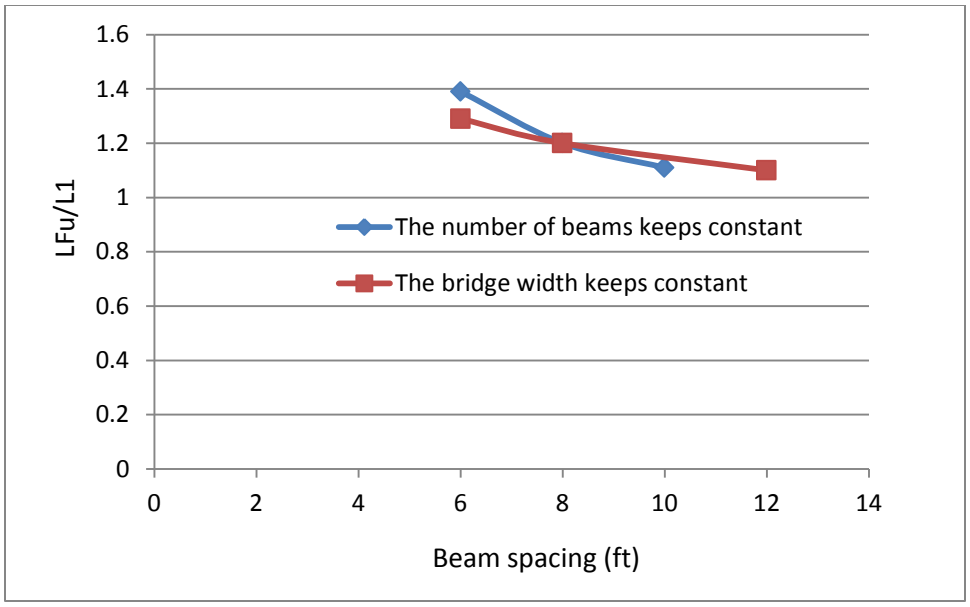

Figure 3.23 Plot of Ru=LFu/LF1 as a function of beam spacing

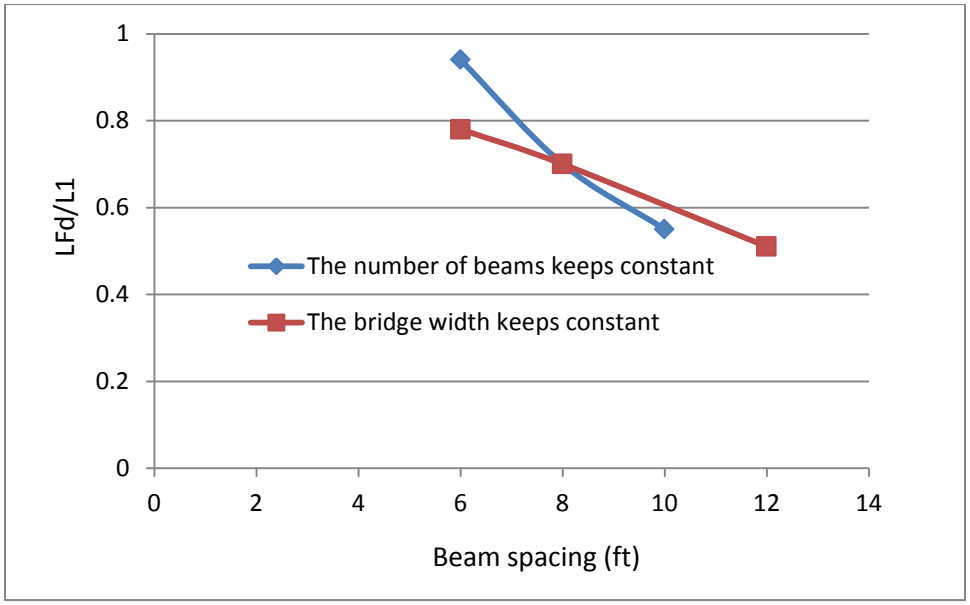

Figure 3.24 Plot of Rd=LFd/LF1 as a function of beam spacing

3.7 Effect of the slab thickness

In the last Quarterly Report, the effect of the reinforcement ratio of the slab was studied and it shows minor effect on the redundancy ratios. Here we go further to investigate the effect of slab thickness as suggested by a reviewer of the last report. The thickness of the slab (the concrete plate above steel girders) is at 7 in. depth for the Base case. Three additional cases are analyzed as follows:

Base case: 7 in. slab thickness;
Case 1: 8 in. slab thickness;
Case 2: 9 in. slab thickness;
Case 3: 10 in. slab thickness;

Moment curvature curves for Cases 1-3 are compared to those of the base case for the composite steel I-girder and the concrete slab in Figure 3.25 and Figure 3.26, respectively. The load deflection curves for the Base case and Cases 1-3 are shown in Figure 3.27. Also, the cross section properties of the composite steel I-girder and the slab are listed in Table 3.14 and 3.15, respectively. The redundancy analysis results are summarized in Table 3.16 & 3.17.

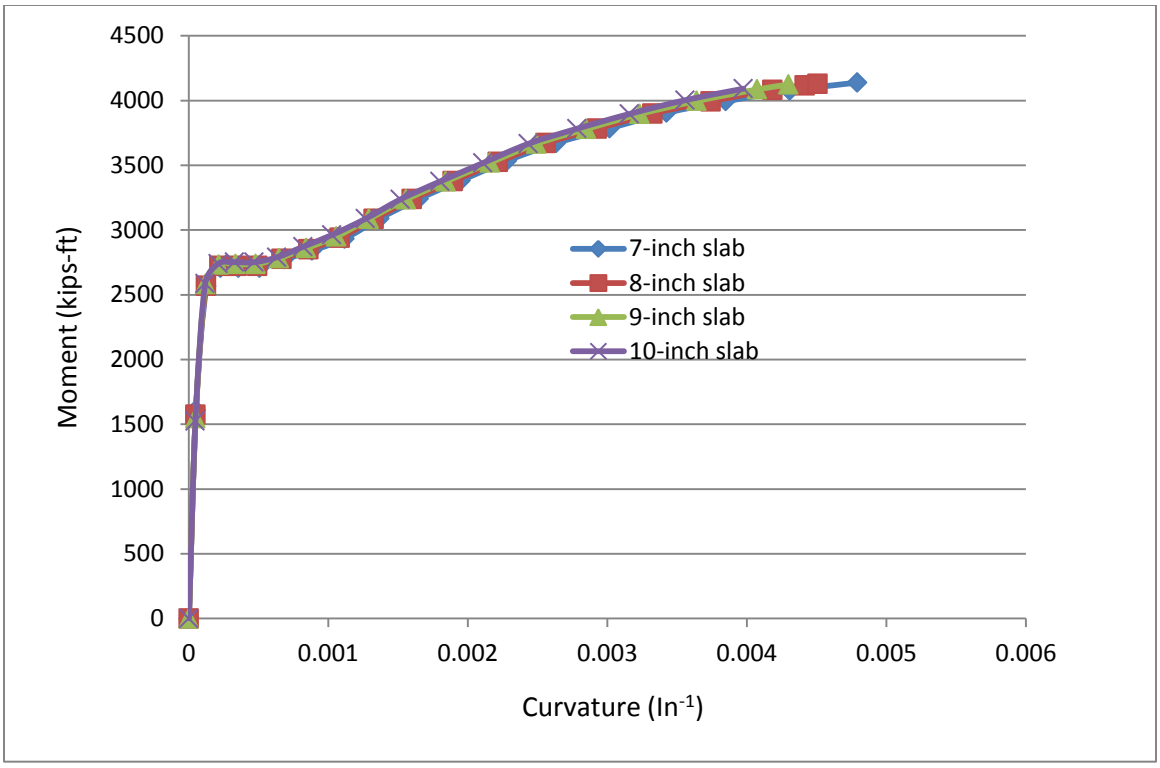

Figure 3.25 Moment-curvatures of composite steel girders for positive moment region

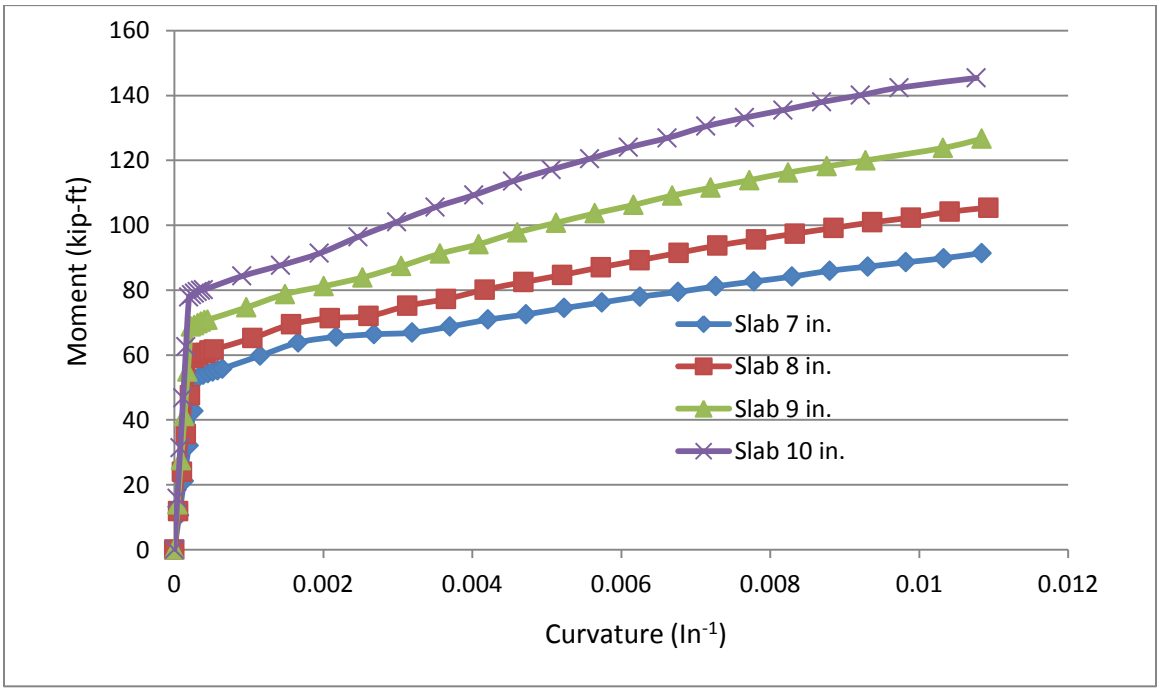

Figure 3.26 Moment-curvature of the concrete slab for the thickness 7-in., 8-in., 9-in. and 10-in.

Table3.14 Gross superstructure properties for positive moment region _ based on steel girder material

Slab thickness	A (ft^2)	I_{xx} (ft^4)	I_{yy} (ft^4)	Weight (pcf)
Base case (7 in.)	1.107	1.30	4.07	786
Case 1 (8 in.)	1.216	1.38	4.65	798
Case 2 (9 in.)	1.324	1.46	5.23	808
Case 3 (10 in.)	1.433	1.54	5.81	816

Table3.15 Gross section properties for the concrete slab

Slab thickness	A (ft^2)	I_{xx} (ft^4)	I_{yy} (ft^4)
Base case (7 in.)	5.83	0.17	48.61
Case 1 (8 in.)	6.67	0.25	55.56
Case 2 (9 in.)	7.50	0.35	62.50
Case 3 (10 in.)	8.33	0.48	69.44

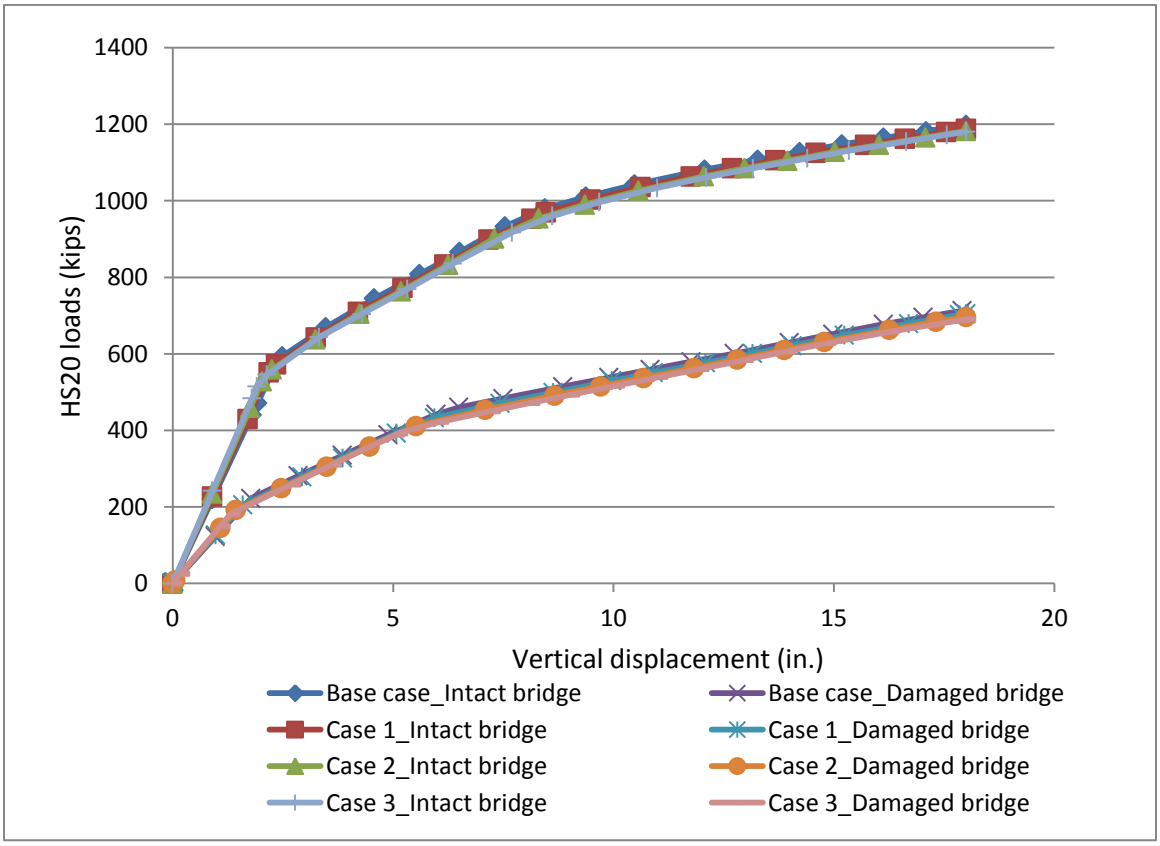

Figure 3.27 Load-deflection curves for the Base case and Cases 1-3

It is observed from Figure 3.25 -3.27 that the moment-curvature curves for the composite girder do not change much as the slab thickness increases. Although the ultimate capacity of the slab increases significantly, the ultimate load factors of LF_u and LF_d have a small change, as shown in Table 3.17.

The parameter changing significantly here is the Load factor LF_1 because the dead load increases a lot as the concrete slab thickness increases from 7 in. up to 10 in., as shown in Table 3.16. The last two column data in Table 3.17 show that the redundancy ratios increase 9% and 10% for the ultimate state and the damage bridge condition, respectively, as the slab thickness only increases about 4%. It is concluded that larger concrete slab thickness leads to higher redundancy ratios for composite steel bridges, but the ultimate load carrying capacity of the bridges does not change.

Table3.16 Comparison of results of redundancy analysis of various slab thicknesses

Slab thickness	R (kip-ft)	D (kip-ft)	LL (kip-ft)	R/D	LF_1
Base case (7'')	4139	405	537.5	10.22	6.95
Case 1 (8'')	4129	456	548.6	9.05	6.70
Case 2 (9'')	4124	507.2	558.1	8.13	6.48
Case3 (10'')	4092	538.4	566.9	7.60	6.27

Table3.17 Comparison of results of redundancy analysis of various slab thickness

Slab thickness	LF_1	LF_u	LF_d	R_u	R_d*
Base case (7'')	6.95	8.32	4.95	1.20	0.71
Case 1 (8'')	6.70	8.25	4.89	1.23	0.73
Case 2 (9'')	6.48	8.21	4.83	1.27	0.75
Case3 (10'')	6.27	8.20	4.79	1.31	0.76

Note: * Weight of damaged beams is included and transferred to the adjacent beam.

4. Conclusions

In this report we continued the sensitivity analysis for the redundancy of the three-span composite steel bridge superstructure under the effect of vertical loads and performed a parametric analysis to identify the primary variables that control the redundancy of such systems. From this analysis, it is observed that the plastic hinge length, bridge bracing and girder stiffness have generally minor effect on bridge redundancy. Moderate changes in member resistances will have some effect on the redundancy ratios which may be on the order of ¼ of the change in member capacity for the ultimate limit state and about ½ for the damaged limit state. The parameter that seems to have most effect is the beam spacing and slab thickness. The number of beams is important only when the beam spacing is small. Larger beam spacing leads to lower bridge redundancy for the ultimate state and even more so for the damaged bridge condition. About 4% increase in slab thickness could raise the bridge redundancy ratios about 10% at the ultimate state and the damaged condition. With regard to truck numbers, the side-by-side trucks in the middle span are more likely to control the redundancy of this type of multi-span bridges. Higher redundancy ratios are observed if a single truck is loaded in each of two spans as compared to the side-by-side trucks in each of two spans. The analysis of the simple span bridges shows insignificant change in the redundancy ratio for the ultimate limit state when the member resistance or the dead load are changed.

5. References

1. Burdette, E. G., and Goodpasture, D. W. (1971). Full-Scale Bridge Testing-An Evaluation of Bridge Design Criteria. Department of Civil Engineering, The University of Tennessee, TN.

2. Ghosn, M., and Moses, F., (1998). Redundancy in Highway Bridge Superstructures. National Cooperative Highway Research Program, NCHRP Report 406, Transportation Research Board, Washington DC: National Academy Press.

3. Hambly EC. (1991) Bridge Deck Behavior. London: Chapman and Hall, Ltd.